A Concise Overview of the Use of Low-Dimensional Molybdenum Disulfide as an Electrode Material for Li-Ion Batteries and Beyond

batteries

MDPI

Review

A Concise Overview of the Use of Low-Dimensional Molybdenum Disulfide as an Electrode Material for Li-Ion Batteries and Beyond

Mattia Bartoli [1,2,3,*], Meltem Babayiğit Cinali [3,4,*], Özlem Duyar Coşkun [4], Silvia Porporato [1,3], Diego Pugliese [3,5], Erik Piatti [3], Francesco Geobaldo [3], Giuseppe A. Elia [1,3], Claudio Gerbaldi [1,3], Giuseppina Meligrana [1,3] and Alessandro Piovano [1,3,*]

1 Center for Sustainable Future Technologies—CSFT@POLITO, Via Livorno 60, 10144 Torino, Italy; silvia.porporato@polito.it (S.P.); giuseppe.elia@polito.it (G.A.E.); claudio.gerbaldi@polito.it (C.G.); giuseppina.meligrana@polito.it (G.M.)
2 National Reference Center for Electrochemical Energy Storage (GISEL)-INSTM, Via G. Giusti 9, 50121 Firenze, Italy
3 Department of Applied Science and Technology (DISAT), Politecnico di Torino, Corso Duca degli Abruzzi 24, 10129 Torino, Italy; d.pugliese@inrim.it (D.P.); erik.piatti@polito.it (E.P.); francesco.geobaldo@polito.it (F.G.)
4 Thin Film Preparation and Characterization Laboratory, Department of Physics Engineering, Hacettepe University, Beytepe, 06800 Ankara, Turkey; duyar@hacettepe.edu.tr
5 National Institute of Metrological Research (INRiM), Strada delle Cacce 91, 10135 Torino, Italy
* Correspondence: mattia.bartoli@polito.it (M.B.); mbabayigit@hacettepe.edu.tr (M.B.C.); alessandro_piovano@polito.it (A.P.); Tel.: +39-011-090-4681 (A.P.)

Abstract

The urgent demand for sustainable energy solutions in the face of climate change and resource depletion has catalyzed a global shift toward cleaner energy production and more efficient storage technologies. Lithium-ion batteries (LIBs), as the cornerstone of modern portable electronics, electric vehicles, and grid-scale storage systems, are continually evolving to meet the growing performance requirements. In this dynamic context, two-dimensional (2D) materials have emerged as highly promising candidates for use in electrodes due to their layered structure, tunable electronic properties, and high theoretical capacity. Among 2D materials, molybdenum disulfide (MoS_2) has gained increasing attention as a promising low-dimensional candidate for LIB anode applications. This review provides a comprehensive yet concise overview of recent advances in the application of MoS_2 in LIB electrodes, with particular attention to its unique electrochemical behavior at the nanoscale. We critically examine the interplay between structural features, charge-storage mechanisms, and performance metrics—chiefly the specific capacity, rate capability, and cycling stability. Furthermore, we discuss current challenges, primarily poor intrinsic conductivity and volume fluctuations, and highlight innovative strategies aimed at overcoming these limitations, such as through nanostructuring, composite formation, and surface engineering. By shedding light on the opportunities and hurdles in this rapidly progressing field, this work offers a forward-looking perspective on the role of MoS_2 in the next generation of high-performance LIBs.

Keywords: 2D material; molybdenum disulfide; Li-ion battery; anode; energy storage

Academic Editors: Torsten Brezesinski and Jianqing Zhao

Received: 16 May 2025
Revised: 18 June 2025
Accepted: 15 July 2025
Published: 16 July 2025

Citation: Bartoli, M.; Cinali, M.B.; Coşkun, Ö.D.; Porporato, S.; Pugliese, D.; Piatti, E.; Geobaldo, F.; Elia, G.A.; Gerbaldi, C.; Meligrana, G.; et al. A Concise Overview of the Use of Low-Dimensional Molybdenum Disulfide as an Electrode Material for Li-Ion Batteries and Beyond. *Batteries* **2025**, *11*, 269. https://doi.org/10.3390/batteries11070269

1. Introduction

The growing demand for efficient and sustainable energy-storage solutions has driven both academic and industrial research to focus on the development of highly engineered

materials. Two-dimensional (2D) materials are layered materials, the thickness of which can be reduced to the nanometer scale (theoretically up to the monolayer, but generally with a thickness spanning from 1 to a few nanometers); this is usually thanks to the weak Van der Waals interactions between layers that enable their facile exfoliation while retaining robust mechanical strength within each layer [1]. In the last two decades, 2D materials have garnered the attention of the scientific community thanks to this ultimate scaling in the 2D limit, where they often exhibit a range of remarkable properties that are absent—or distinct—from those of their bulk counterparts. Prior to this recent surge of interest, bulk-layered materials had been extensively investigated for various applications in catalysis and lubrication [2]; however, the experimental realization of monolayer graphene sparked a tremendous amount of research activity toward the exploration of the exotic phenomena arising from its linearly dispersing energy bands and massless Dirac fermions [3]; moreover, its exceptionally high room-temperature electron mobility (>50,000 cm^2 $(V \cdot s)^{-1}$) has naturally motivated applications in high-speed electronic devices [4].

There are many production routes for 2D materials, which can be grouped in two categories: bottom–up and top–down [5]. The bottom–up approaches (chemical and physical vapor deposition) are the best performing for the production of high-quality materials but they are hard to scale-up at very large scale [6,7], with the exception of templated wet synthesis. Templated synthesis is quite interesting both for scale-up and tunability, but it requires very efficient purification post-synthesis steps [8]. The top–down routes (i.e., exfoliations [9] or grinding [10]) are easy to scale-up, but their outputs are not as good as the materials obtained from bottom–up routes in terms of controlled size and morphology [11].

Beyond the graphene family of materials [3,4,12], the most studied and widely explored 2D materials for electrodes are layered transition metal dichalcogenides (TMDs) [13–15], such as molybdenum disulfide (MoS_2), but also extend to post-transition metal chalcogenides (e.g., InSe and Bi_2Se_3) [16,17], 2D carbides or MXenes (e.g., Ti_3C_2 and Nb_2C) [18], layered dihalides and trihalides (e.g., PbI_2 and CrI_3) [19,20], 2D oxides (e.g., MoO_3) [21], perovskites [22], and 2D elemental materials, including silicene [23] and black phosphorus [24]. Amongst these, MoS_2 has emerged as a promising candidate for battery applications due to its unique layered structure, high theoretical capacity, and tunable electronic properties [25]. Particularly, low-dimensional MoS_2 has gathered a great deal of attention due to its electrochemical performance and structural stability [26]. With respect to more conventional 3D materials, the understanding of electronic transport and carrier dynamics in 2D materials is significantly complicated by the extreme anisotropy intrinsic to their crystal structure and their large compositional and structural variability [27]. Beyond the obvious consequences arising from their chemical composition, some of the main aspects affecting electronic transport in 2D materials are structural polymorphism; the number of layers composing the material; the electronic coupling between different layers; sources of scattering, including structural and/or chemical disorder; the environment in which the material is embedded; and the contact resistance against carrier injection in the 2D material [28].

The extreme chemical richness of 2D materials, enabled by the wide palette in both their chemical composition and available crystal structures, results in an incredible variety of different electronic properties in this family of materials, ranging all the way from wide-band-gap insulators such as hexagonal boron nitride [29], to Dirac semimetals such as graphene [30], superconductors such as $NbSe_2$ [31], and topological insulators such as Bi_2Se_3 [27]. Overall, the diversity of electronic properties in 2D materials offers numerous opportunities in the fields of electronics and optoelectronics, catalysis, chemical and biological sensing, electrochemistry, energy storage, CO_2 splitting, and hydrogen evolution [17,32]. As shown in Figure 1, the application of MoS_2 in LIBs has received increasing attention

from the scientific community in recent years, while the number of review and perspective articles has remained rather poor, thus limiting the overall vision on this topic. Accordingly, in this concise review, we are focusing on MoS_2, offering an overview on some of its key features and the most relevant and best performing solutions for facing the most intriguing challenges in its use as an electrode for Li-ion battery (LIB) applications, with some recent and future trends to guide innovative research in the field. This will provide a handy benchmark for experts and newcomers.

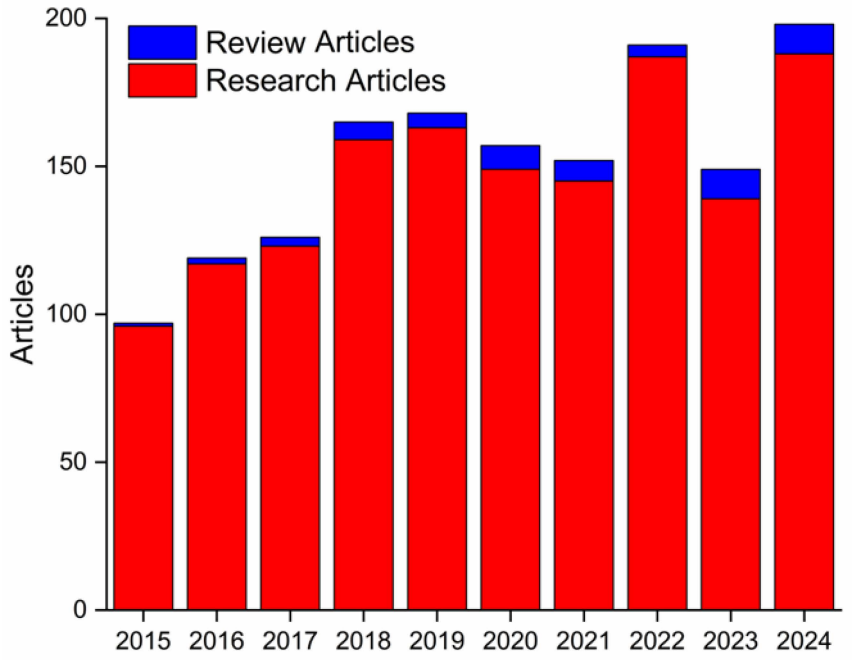

Figure 1. Number of original research and review articles published from 2014 until 2024 as reported in the Scopus database using the search keywords "MoS_2" and "Lithium batteries".

2. An Overview of Key MoS_2 Properties

MoS_2 is widely recognized for its excellent lubricating performance, which is largely due to its layered crystal structure and inherently low friction coefficient [2]. This material demonstrates superlubricity—a phenomenon whereby the shear strength increases concurrently with the coefficient of friction. Measurements of MoS_2's friction coefficient and shear strength across various environments yielded values of 0.150 (evaluated) and 56.0 MPa (estimated), respectively, under standard ambient conditions [26]. The tribological performance of MoS_2 can be further enhanced through chromium (Cr) doping. Microindentation tests on Cr-doped MoS_2 nanopillars revealed a rise in yield strength from 821 MPa (undoped) to 1017 MPa at a 50% Cr concentration [33]. The increase in mechanical strength also corresponds to a shift in failure behavior—from ductile bending in pure MoS_2 to brittle fracture in Cr-doped structures.

In the context of flexible electronics, the mechanical characteristics of MoS_2 have become the subject of intensive research. Monolayer MoS_2 exhibits notable tensile strength (albeit inferior to graphene) and elasticity comparable to that of graphene oxide, with a reported Young's modulus of 0.33 ± 0.07 TPa [34]. Unlike conventional semiconductors, MoS_2 maintains its crystalline structure under mechanical strain, avoiding deformation and band-gap shifts. Nonetheless, strain engineering is actively used to tune its electronic properties, transforming it from a semiconductor to a conductor by converting the direct band-gap of the monolayers into an indirect one. High levels of strain can close the band-gap, resulting in metallic conduction [35]. Using atomic force microscopy, nanoscale bending experiments on exfoliated MoS_2 flakes deposited on perforated substrates esti-

mated the yield strength to be 270 GPa for monolayers [36] and 330 GPa for multilayer flakes [37].

Optically, MoS_2 demonstrates high absorption in the 400–500 nm spectral range, followed by a steep decline past 500 nm [38]. Its band-gap tunability to thickness and structure underlies its prominence in optoelectronic devices, enabling customized photoresponsivity, detectivity, and response times [39]. The refractive index, which exceeds 2 for both single and multilayer forms, supports its role in advanced photonic applications. Photoluminescence (PL) varies depending on the band-gap, doping, and structural configuration. Monolayer MoS_2 exhibits distinct PL peaks at approximately 630 and 670 nm, which are associated with B and A excitons, respectively. Treatment with hydrogen peroxide has been shown to enhance PL without altering the crystal structure [40]. Although TMDs typically suffer from low PL quantum yield (QY) values, ranging from 0.01 to 6%, chemical treatment using an organic superacid led to an increase in MoS_2's QY to 95% [35]; alongside a measured carrier lifetime of about 10.8 ns, this highlights its potential in laser and photovoltaic technologies.

In its multilayer form, MoS_2 has an indirect band-gap of 1.2 eV, which transitions to a direct band-gap of 1.8 eV as the layer count is reduced to a monolayer [41]. As previously mentioned, mechanical strain can induce a direct-to-indirect band-gap transition, modulating its electronic character. The electronic behavior of MoS_2 is primarily governed by interactions between the molybdenum 4d and sulfur 3p orbitals. While the projected density of states (PDOS) is similar for both bulk and monolayer MoS_2, the monolayer's PDOS features sharper peaks, unlike the broader distribution observed in bulk material [42]. Doping MoS_2 alters its electronic type: chromium (Cr), copper (Cu), and scandium (Sc) induce n-type behavior, whereas nickel (Ni) and zinc (Zn) produce p-type characteristics [43]. Titanium (Ti) doping, depending on both the concentration and site (interstitial or substitutional), can yield p-type, n-type, or half-metal properties [44]. For instance, at a 2.04% doping level, interstitial Ti results in p-type behavior [45]; at 3.57%, n-type behavior is observed due to stronger covalent bonding and an increased surface dipole that reduces the electron affinity to 0.49 eV. At a 7.69% Ti content, MoS_2 becomes a ferromagnetic half-metal with full spin polarization. Interestingly, substitutional Ti doping across the same concentrations does not significantly impact MoS_2's electronic profile.

Bulk MoS_2 has garnered attention as an anode material for LIBs owing to its unique capacity to accommodate Li^+ through both intercalation and conversion mechanisms, achieving a high lithium storage capacity of roughly 670 mAh g^{-1}, which is nearly double that of graphite (the standard LIB anode) [46]. However, limitations such as poor electrical conductivity, slow lithium diffusion, and structural instability during cycling hinder its practical use. These challenges can be addressed through nanostructuring approaches, such as producing MoS_2 in forms like nanosheets, quantum dots, nanoflowers, nanotubes, and heterostructures, which offer increased surface area, shortened diffusion paths, and enhanced mechanical stability [47].

As nanotechnology and spintronics evolve, understanding the spin dynamics in MoS_2 has become increasingly important. Although TMDs are intrinsically non-magnetic, introducing magnetic properties is key to their use in spin-based electronic applications [48]. Research by Tongay et al. [49] revealed that single-crystal MoS_2 exhibits a mix of diamagnetic and ferromagnetic responses under magnetic fields of up to 5 T and temperatures down to 10 K. The observed ferromagnetism is attributed to structural features such as zigzag edges at the grain boundaries and sulfur vacancies. Given the minimal interlayer magnetic coupling, these findings are likely limited to monolayers. Complementary studies on multilayer MoS_2 by Liang et al. [50] report a substantial spin diffusion length of 235 nm and note that in-plane spin polarization effectively reduces spin relaxation. The intrinsic

electronic structure of low-dimensional MoS_2 supports its candidacy for electrochemical applications [51].

Crystal-phase polymorphism plays a crucial role in 2D materials like MoS_2, where small phase variations lead to significant changes in their electronic behavior, ranging from metallic to semiconducting or even superconducting [52–54]. Layer thickness also greatly influences electronic characteristics such as band-gaps and plasmon frequencies due to quantum confinement effects [16,55]. Charge carrier mobility is often degraded by scattering, which may originate from intrinsic factors (electron–phonon and electron–electron interactions) or extrinsic ones (structural defects, surface roughness, Coulomb interactions, or substrate phonons) [56,57]. Given the large surface-to-volume ratio and poor electrostatic screening of 2D systems, the surrounding environment—particularly the substrate—has a marked impact on electronic performance. This environmental sensitivity is critical in determining *intra*-layer transport, while *inter*-layer transport is shaped by the coupling between adjacent layers. Weak Van der Waals interactions act as tunneling barriers, creating significant anisotropy in carrier mobility [58]. Additionally, charge injection into 2D materials, which is often hampered by contact resistance at interfaces with metals, can be a bottleneck. Factors like energy-band alignment, interface transparency, and the presence of tunneling barriers all play a role [59,60]. Similar considerations apply to composite structures of 2D flakes, where the nature of *inter*-flake contacts dictates whether transport is diffusive or hopping-dominated [61,62]. These multifaceted transport characteristics must be carefully evaluated when integrating 2D materials like MoS_2 into functional electronic systems.

3. On the Use of MoS_2 as a Li-Ion Battery Anode

MoS_2 is under investigation for its potential use as an electrode material in various battery chemistries, chiefly in lithium–sulfur (Li-S) and beyond lithium-ion technologies, as well as in supercapacitors [63]. The main limitations in the utilization of low-dimensional materials such as 2D-MoS_2 in commercial devices are related to their cost, which still remains high at up to thousands of USD/g [64]. Furthermore, the absence of shared standard practices for their production and characterization has risen doubts and slowed their entry into the market. Nevertheless, nanosized MoS_2 can match the performances of few-layered MoS_2, considerably reducing the price [65]. As reported by Tao et al. [66], nanomaterials can be combined with advanced manufacturing techniques to improve overall LIB production. Fang et al. [67] discussed the readiness of MoS_2-based LIBs to be commercialized in the near future, highlighting cost and stability as issues to be properly addressed than a major breakthrough can be reached. As reported by Bisset et al. [68], MoS_2-based aqueous supercapacitors in the form of coin cells at the laboratory-scale can be implemented using sodium sulphate as an aqueous electrolyte and graphene-containing membranes. The combination of these elements increased the specific capacity (through an intercalation/pseudo-capacitance mechanism), proving the feasibility of layered 2D MoS_2 for practical uses. Conversely, pouch-cell-based set-ups have been used more for other chemistries, including for lithium sulfur [69,70], potassium [71], and calcium [72].

Low-dimensional MoS_2 has gained attention for battery applications due to some unique features that are related to both its morphological and electronic properties. Considering lithium-based systems, Li diffusion into bulk MoS_2 is hindered by the interlayer spacing of up to 0.62 nm, while few-layered MoS_2 shows expanded interlayer spacing with a significant reduction in the energy barriers for Li insertion [73,74]. MoS_2 heterostructures can further boost mobility, partially compensating for the poor electrical conductivity. Accordingly, MoS_2 has been widely used for applications in LIBs using several routes as shown in Table 1, including mixing with carbon-based species such as graphene oxides

(GO), reduced GO (rGO), single- and multiwalled carbon nanotubes (SWCNTs, MWCNTs), and inorganics.

Table 1. Overview of research studies focused on the utilization of MoS_2 in LIBs.

Material	Specific Capacity (mAh g^{-1})	Coulombic Efficiency	Reference
Amorphous bulky MoS_2	100	54% after 100 cycles	[75]
Nanoflake MoS_2	1175	96% after 40 cycles	[76]
Cobalt-templated few-layered MoS_2	1661	92% after 300 cycles	[77]
Lysine-templated few-layered MoS_2	1160	51% after 70 cycles	[78]
Plasma-treated MoS_2	1038	50% after 70 cycles	[79]
Nitrogen-doped MoS_2	1130	86% after 100 cycles	[80]
Stacked 2D MoS_2	569	90% after 200 cycles	[81]
Vertically aligned MoS_2 nanotubes	1100	83% after 200 cycles	[82]
Mesoporous silica-templated 1T-MoS_2	1100	80% after 50 cycles	[83]
3D self-assembled few-layered MoS_2	1137	54% after 50 cycles	[84]
MoS_2 nanotubes	1253	16% after 50 cycles	[85]
MoO_3@MoS_2	564	99% after 50 cycles	[86]
MoO_3@MoS_2	864	39% after 1000 cycles	[87]
MoO_3@MoS_2	1531	78% after 100 cycles	[88]
Core–sheath MoO_3@MoS_2	1531	98% after 150 cycles	[89]
ZnS@MoS_2	1346	73% after 300 cycles	[90]
TiO_2@MoS_2	827	73% after 100 cycles	[91]
TiO_2@MoS_2	871	54% after 80 cycles	[92]
SnO_2@MoS_2	530	75% after 150 cycles	[93]
SnO_2@MoS_2	707	71% after 100 cycles	[94]
$CoMoO_4$@MoS_2	1100	55% after 100 cycles	[95]
Co_3O_4@MoS_2	1200	67% after 100 cycles	[96]
VS_2@MoS_2 *	585 *	n.a. *	[97]
MoS_2@MWCNTs	1214	85% after 60 cycles	[98]
MoS_2@SWCNTs thin film	1066	93% after 60 cycles	[99]
MoS_2@MWCNTs layered composites	670	75% after 80 cycles	[100]
TiO_2@MoS_2@MWCNTs	680	85% after 200 cycles	[101]
MoS_2 supported on graphene	877	62% after 60 cycles	[102]
MoS_2 supported on a few layers of graphene	1229	77% after 60 cycles	[103]
MoS_2 supported on graphene aerogel	1140	91% after 60 cycles	[104]
MoS_2 supported on graphene cryo-aerogel	863	~99% after 60 cycles	[105]
Vertically aligned MoS_2 supported on GO	1077	87% after 400 cycles	[106]
Nanoflowers of MoS_2 supported on rGO	1250	54% after 250 cycles	[107]
Nanoflowers of MoS_2 supported on rGO	1150	77% after 60 cycles	[108]
MoS_2 supported on graphdiyne oxide	653	~99% after 600 cycles	[109]
MoS_2 supported on nitrogen-doped graphene	1040	97% after 100 cycles	[110]

Table 1. *Cont.*

Material	Specific Capacity (mAh g^{-1})	Coulombic Efficiency	Reference
MoS_2 supported on nitrogen-doped graphene	727	97% after 100 cycles	[111]
2D MoS_2 supported on carbon nanosheets	709	95% after 520 cycles	[112]
MoS_2 supported on amorphous carbon	521	~99% after 100 cycles	[113]
MoS_2 incorporated into carbon spheres	1813	~99% after 100 cycles	[114]
MoS_2 incorporated into carbon sponges	784	86% after 100 cycles	[115]
MoS_2 incorporated into carbon nanocages	1372	91% after 100 cycles	[116]
MoS_2 supported on poly(dopamine)	1210	~99% after 100 cycles	[117]
MoS_2 supported on poly(aniline)	888	97% after 100 cycles	[118]

(*) value obtained based on DFT calculation.

LIBs are the most widely used energy-storage devices due to their high energy density, long cycle life, and relatively high power density [119]. First commercialized by Sony in 1991, LIB functioning mainly relies on the reversible movement of Li^+ ions between the graphite (generally referred to as its lithiated form Li_xC_6) anode and the layered oxide ($Li_{1-x}T^MO_2$) cathode, thus allowing for reversible energy conversion (i.e., the process of transformation of stored chemical energy into electrical energy) and storage. Here, T^M refers to a transition metal; while cobalt is the most extensively researched T^M material, other transition metals such as nickel and manganese are also commonly used [120,121]. At present, graphite is the most popular anode electrode material in commercially produced LIBs because it has good cycling stability as well as being an abundant and inexpensive natural resource [122–125]. In graphite anodes, lithium ions are intercalated between the graphene layers, with one lithium atom per six carbon atoms, and the resulting fully lithiated graphite (LiC_6) has a theoretical specific capacity of 372 mAh g^{-1}. However, this capacity value of graphite anodes is insufficient to meet the higher energy and, particularly, power requirements of current and future technologies such as advanced electric vehicles [122,123,125–128]. In addition, when graphite is used as the anode material in LIBs, the slow interface kinetics causes the anode voltage to drop to below 0 V vs. to Li^+/Li under fast charging conditions, thus coating the graphite surface with metallic lithium [129]. The typical morphology of Li dendrites corresponds to the branched or tree-like structures of the Li metal, in which Li ions are not homogeneously deposited onto the anode surface but form random protuberances on it [130]. The formation of dendrites causes a significant loss of capacity during high-speed cycling, as well as burning, and even exploding, LIBs due to short-circuits [129]. For these reasons, scientific studies on the development of new anode materials that can be used in LIBs are very important [131]. Among the many alternative anode materials, MoS_2, the theoretical specific capacity of which is almost twice than that of graphite, has been extensively investigated as an anode material for LIBs [132–134]. The reaction pathways that may occur in the use of MoS_2 in LIBs are given in Figure 2.

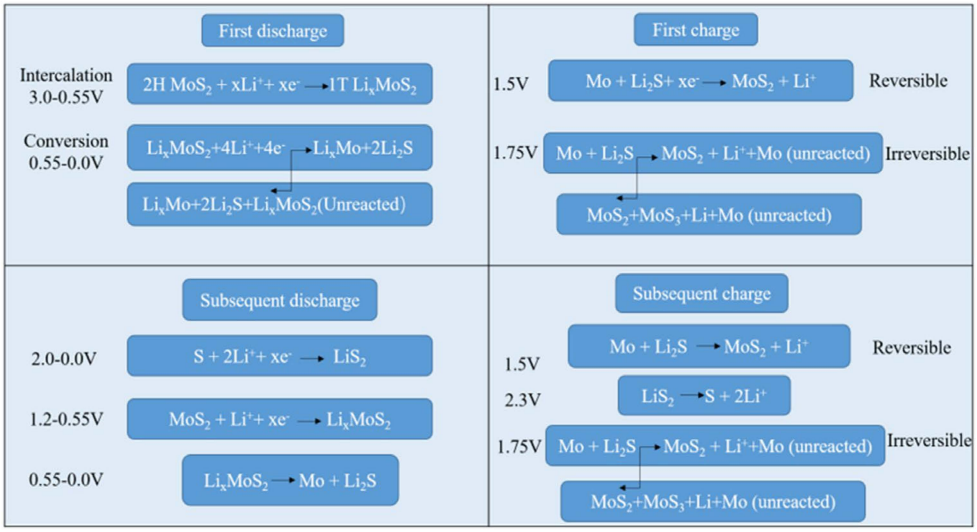

Figure 2. Reaction pathways occurring at the MoS_2 anode in LIBs. Reprinted with permission from Zhao et al. [135] (Copyright © 2024 Elsevier).

During discharge, Li ions intercalate the MoS_2 due to the layered structure of MoS_2 assembled through weak Van der Waals forces. Accordingly, the insertion/extraction of Li^+ ions is very easy during the first charge/discharge process [134], preserving the structure and producing a moderate and stable capacity, while further lithiation induces the formation of Mo and Li_2S. This phenomenon significantly improves the capacity but simultaneously causes volume expansion and structural instability [25], as directly observed by in situ TEM by Zeng et al. [136] (Figure 3).

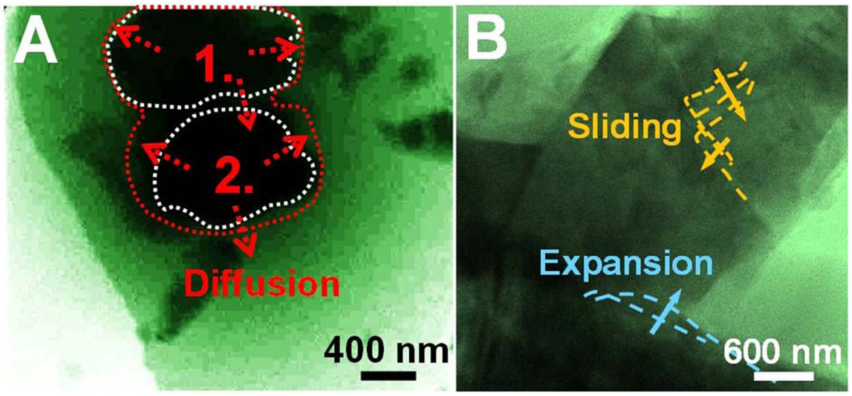

Figure 3. TEM analysis of the (**A**) diffusion and (**B**) structural modification of MoS_2 during the discharge/charge process. Reprinted with permission from Zeng et al. [136] (Copyright © 2015, American Chemical Society).

During the charging process, Li is extracted, restoring the MoS_2 structure, but this process is not fully reversible, leading to gradual capacity loss over multiple cycles [137]. Restructuring MoS_2 into nanoflowers, nanofibers, nanosheets, and nanospheres enhances its structural features by increasing the interlayer spacing and enlarging the surface area. These modifications facilitate Li^+ intercalation and provide more active sites for the conversion reaction [126].

Going down to the atomic scale, the lithiation mechanism of MoS_2 is quite complex, as shown in Figure 4.

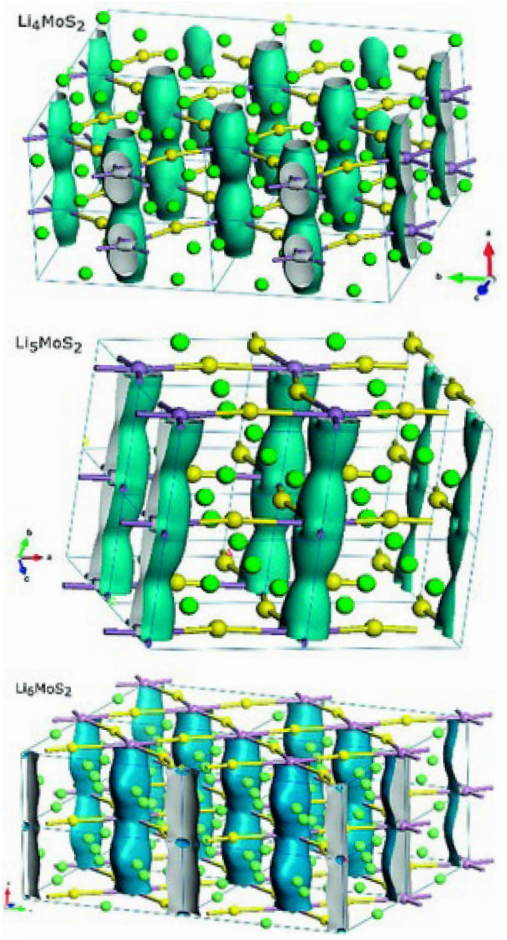

Figure 4. Structural overview of MoS_2 showing the changes under different degree of lithiations. Reprinted with permission from Caputo et al. [138] (Copyright © 2018 Wiley).

As reported by Caputo et al. [138], MoS_2 undergoes lithiation to form Li_xMoS_2 (x = 4, 5, 6), in which the Mo-Mo rich planes are deformed by the presence of Li^+ insertion. Accordingly, the overall lithiation process introduces several local lattice sides around the Mo atoms. Interestingly, the structure changes from trigonal prismatic coordination in $Li_{0.5}MoS_2$ to octahedral coordination in $LiMoS_2$, and reaches a mix of octahedral and trigonal prismatic coordination in $Li_{1.5}MoS_2$, which turns back to an octahedral arrangement in Li_2MoS_2 [139]. These relevant morphological and crystal transitions deeply affect both the mobility of Li^+, limiting the lithiation process, and change the MoS_2 energy of the valence band accordingly [140], while other dichalcogenide metal low-dimensional materials such as NbS_2 and ZrS_2 promote intercalation as the preferred lithiation process [141]. Additionally, the discharge process involves a complex pathway that induces the formation of amorphous MoS_2 nanograins, contrary to the obsolete mechanism that leads the production of Mo and S as fully delithiated products [142]. As reported by Py et al. [143], lithium intercalation drastically increases the electronic energy of the semiconducting host by charge transfer. This phenomena was also observed by the insertion of bigger species, such as sodium, as reported by Cook et al. [144].

The other key feature that should be considered is MoS_2 polymorphism. The polymorphs of single-layer and low-dimensional MoS_2 are the hexagonal-phase 2H and the metastable trigonal prismatic 1T, which are in the semiconductor and metallic phases, respectively [145]. As shown in Figure 5, the diffusion of lithium species through these different phases is characterized by different energetic barriers of lithium migration, with an energy gap of ~0.5 and ~0.3 eV for 2H (Figure 5C) and 1T (Figure 5D), respectively.

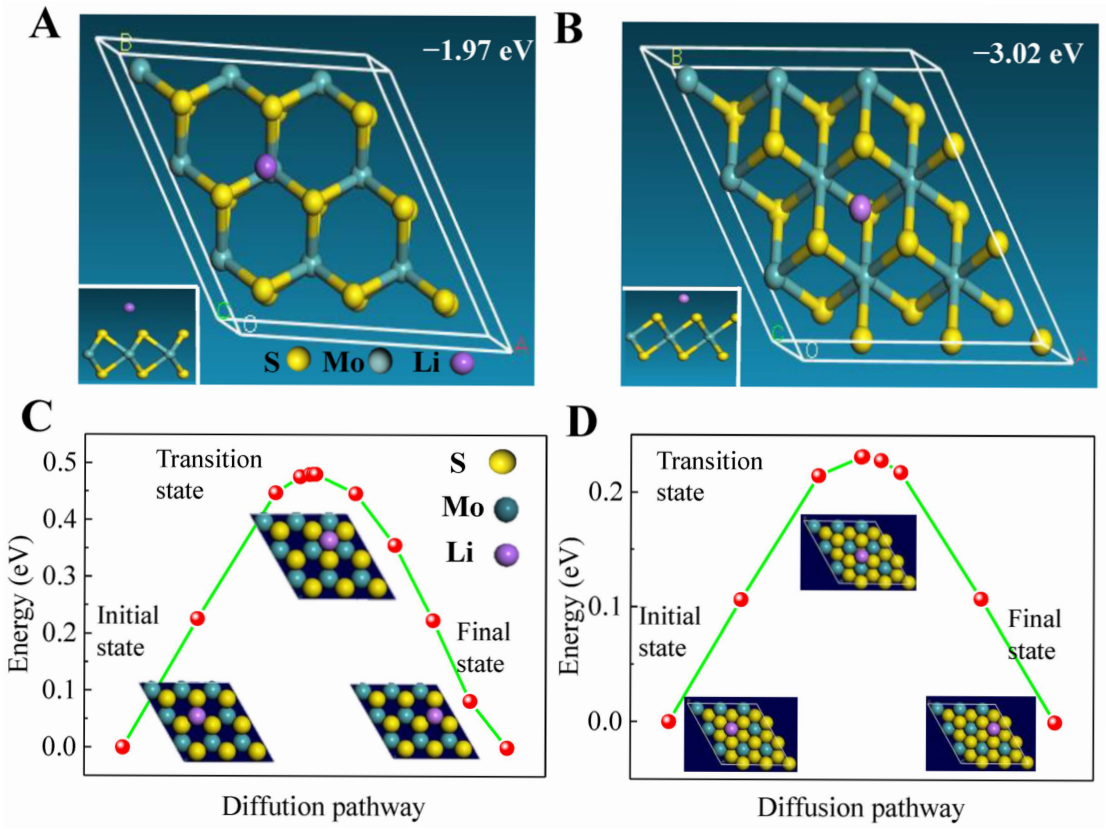

Figure 5. Insertion of Li and related energetic pathways into the 2H (**A**,**C**) and 1T (**B**,**D**) phases. Reprinted with permission from Wang et al. [146] (Copyright © 2012 Royal Society of Chemistry).

Furthermore, the electrochemical performance of MoS_2 in LIBs is determined not only by the bulk processes of insertion and de-insertion of Li ions but also by surface phenomena taking place at the interface between the electrode and the electrolyte. In particular, of great relevance is the formation of the solid–electrolyte interphase (SEI), which is a passivation layer forming spontaneously on the anode surface during the initial charging cycles due to the reductive decomposition of the electrolyte [147]. SEI plays a critical role in the long-term performance and stability of the battery by preventing continuous electrolyte breakdown while allowing lithium-ion transport (as deeply discussed by Zeng et al. [136]). SEI stability is essential for maintaining the capacity and cycling performance of the battery, and a thick SEI can hinder lithium-ion diffusion and increase cell impedance. Yu et al. [148] suggested optimizing the SEI formation by incorporating stabilizing agents in the electrolyte composition and by mixing MoS_2 with carbon fibers, thus achieving improved efficiency of the LIB anode.

As reported by Kan et al. [145], lithiation induces an additional level of complexity to the MoS_2 interplay, as shown in Figure 6, in which the increment in lithium induces a significant distortion of both the H and T phases, promoting the creation of sub-phases with distorted geometries.

Phase control is not the only method to finely tune MoS_2 activity, as reported by a very seminal study by Miki et al. [75], in which bulky amorphous MoS_2 showed the highest specific capacity of 100 mAh g^{-1} with good stability after 100 reversible cycles. Since then, the scientific community has focused its research on engineering and optimizing the MoS_2 morphology to enhance its electrochemical performance. Feng et al. [76] produced MoS_2 nanoflakes that exhibited an increased gravimetric capacity of up to 1175 mAh g^{-1} with a retention of 95% after 40 cycles. Similarly, Wu et al. [78] produced expanded MoS_2 worm-like structures that showed an initial capacity of up to 1161 mAh g^{-1} but a great decrement

down to 585 mAh g^{-1} after only 70 cycles of charge and discharge. The instability of such materials opened the way to the exploration of new optimization/functionalization routes, including heteroatom doping, as reported by Liu et al. [79], which used oxygen plasma to sensibly improve the electrochemical performance of neat MoS_2. Alternatively, Liu et al. [80] unveiled the effect of nitrogen doping in MoS_2, increasing the gravimetric capacity by over 14% over neat material with also an enhancement in coulombic efficiency (CE).

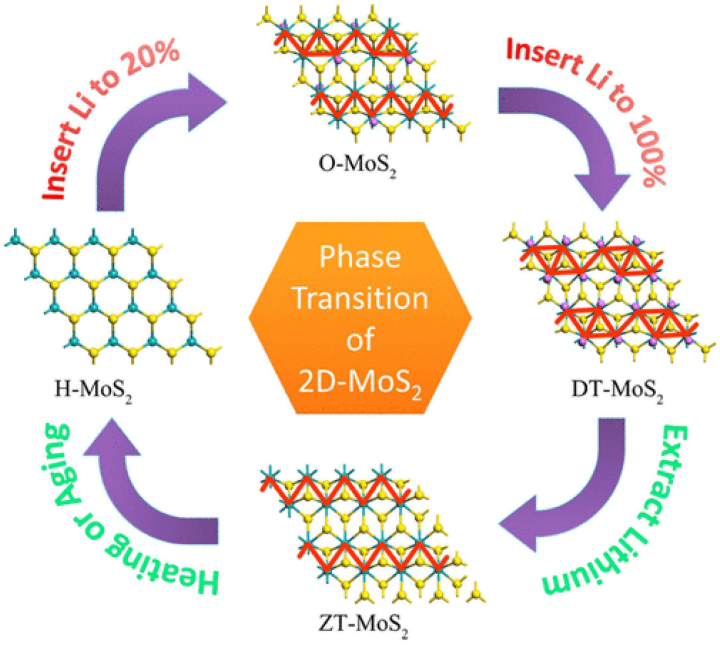

Figure 6. Phase transition of low-dimensional MoS_2 during the lithiation process. Reprinted with permission from Kan et al. [145] (Copyright © 2014 American Chemical Society).

Nevertheless, a more impressive advancement in MoS_2-based LIBs has been the introduction of low-dimensional materials, as reported by Han et al. [77]. The authors modulated MoS_2 assembly using high pressure and cobalt addition to regulate the interspacing distance, achieving a first-charge capacity of 1513 mAh g^{-1} with a CE of 75%, of which 25% was due to irreversible solid electrolyte interphase (SEI) formation, and also demonstrating a stable high capacity even after prolonged cycling for 300 cycles at 0.1 A g^{-1}. The authors suggested that this effect was due to the interfacial storage of lithium ions that promoted the amorphization of active materials. Alternatively, the utilization of different molecular architectures has been explored through the production of highly ordered vertically stacked MoS_2, with a CE up to 90% after 200 cycles, as reported by Sun et al. [81]. Similarly, Jiao et al. [149] produced a metal-like material composed of aligned MoS_2 nanotubes with an excellent reversible capacity of 1100 mAh g^{-1}. The authors reported that their morphology and metallic behavior avoid the use of a conductive additive, promoting electrolyte transportation and diffusion without the restacking of MoS_2 nanosheets together with enhanced cycling stability. Zhao et al. [85] proved that the high crystallinity of MoS_2 nanotubes is critical for its cyclability. The authors produced amorphous MoS_2 nanotubes with an initial specific capacity of 1253 mAh g^{-1} that decreased rapidly to 15% after 50 cycles. Venkateshwaran et al. [83] investigated the pure-phase effect on MoS_2 performance. The authors used a templated approach to produce a stable 1T-MoS_2 with a high specific capacity of 1100 mAh g^{-1} and a capacity retention of 80% after 50 cycles, while other routes allowed a self-assembling of MoS_2 monolayers into 3D structures using a wet-chemistry route [84].

Nevertheless, neat MoS_2 electrodes show unneglectable drawbacks, including poor electrical conductivity and structural degradation along several charge-discharge cycles, as shown in Table 1. These originate from the physical properties of MoS_2, particularly from the weak interlayer interactions due to Van der Waals forces that beneficially boost lithium ion intercalation but contribute to instability under the strain of continuous cycling [150]. Furthermore, the hindered electron transport across the MoS_2 layers significantly decreases their effectiveness during high-rate charge and discharge processes.

Accordingly, the utilization of hybrid solutions has become very attractive for enhancing the durability of MoS_2 [151]. Indeed, the incorporation of other inorganic species represents a solid pathway to mitigate this weakness of MoS_2 by leveraging the strengths of both components. Generally, they form a supporting phase for MoS_2 layers, preventing the volume expansion and contraction that occur during lithiation and delithiation. This structural reinforcement reduces the mechanical stress, which helps to maintain electrode integrity during cycling and improves the overall cycling stability of the system [152]. The simplest approach is represented by the phase engineering of hybrids with molybdenum oxide at the surface and sulfide at the core, as reported by Faizan et al. [86]. The authors combined MoO_3 with MoS_2 by a simple calcination at 300 °C, which resulted in a stable capacity of about 564 mAh g^{-1} while allowing for a greatly enhanced CE up to over 99% after 100 cycles at 0.7 mAh. They suggested that this increased stability is attributed to the formation of a MoO_3 passivation layer on the surface of MoS_2 together with a reactive interface between the two phases, which positively affects the reversible Li^+ storage. Zhao et al. [87] used the very same materials (just tuning their external shapes) to achieve a high capacity of 864 mAh g^{-1} at 0.1 A g^{-1} with good capacity retention, resulting in 336 mAh g^{-1} after 3000 cycles at 2.0 A g^{-1}. Lei et al. [88], using a wet approach for the preparation of the very same materials, achieved a capacity retention of 78% after 100 cycles at 0.2 mAh g^{-1}. Even better results were obtained by Zhao et al. [89], who produced a core–sheath structure with a specific capacity of 1530 mAh g^{-1} and a CE exceeding 98% after 150 cycles. The authors suggested that the improved performance was due to the ability to reduce volume changes during the cycling processes. Similar results were obtained using different metal species (i.e., ZnS [90], TiO_2 [91,92], SnO_2 [93,94], Co clusters [95,96], and VS_2 [97]).

Carbon-hybrid materials represent an alternative and a quite effective solution for enhancing the electrochemical properties of MoS_2-based electrodes, e.g., by using high-tech species such as graphene and related materials, carbon nanotubes (CNTs), or templated carbon [153].

Carbon nanotubes (CNTs) are able to create excellent electrical conductivity pathways across MoS_2, while their morphology promotes better ion penetration and diffusion. MoS_2 anchored or embedded within a CNT network is generally able to retain its structure, with an increase in the cycling stability and rate capability under high current densities. The first example of this was reported by Bindumadhavan et al. [98], using multiwalled CNTs (MWCNTs) added to the electrode by a simple dry-grinding procedure. The authors achieved an initial charge capacity of 1214 mAh g^{-1} with 85% retention after 60 discharge–charge cycles at a current density of 0.5 A g^{-1}. Wang et al. [99] used single-walled CNTs (SWCNTs) for the preparation of hybrid thin films with an average thickness of 1 µm. The authors reported a reduction in the original capacity of SWCNTs compared with MWCNTs but superior retention properties after 60 cycles, reaching up to 93%. Furthermore, degradation of the morphology of the SWCNTs-based composites was reported only after 100 cycles, while a neat MoS_2 thin-film analog displayed significant cracks. Yoo et al. [100] proposed an alternative layer-by-layer approach in which MoS_2 was deposited onto a

MWCNT carpet, despite not achieving comparable results for cyclability and reversibility. Furthermore, an inorganic–CNT mix could be also produced with improved results [101].

The integration of MoS_2 with graphene and related materials improves the electrical conductivity of MoS_2, compensating for the low values of neat MoS_2 [126] and improving the ion mobility, as shown in Figure 7.

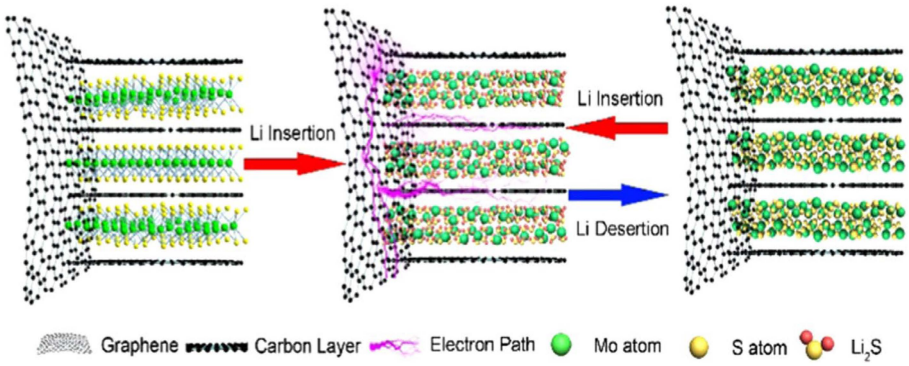

Figure 7. Improving lithium insertion and de-insertion using MoS_2 mixed with graphene. Reprinted with permission from Wang et al. [154] (Copyright © 2017 Elsevier).

This is ascribed to the interaction between the two materials, which are often grown one on the other with strong interfacial contact. This tight interaction reduces charge-transfer resistance at the interfaces, supporting the rapid migration of Li^+ during lithiation and delithiation and enhancing the overall reaction kinetics with a uniform charge distribution across the electrode. Furthermore, graphene and related materials improve the mechanical and structural integrity of MoS_2 by preventing the stacking of MoS_2 layers. This induces an increase in porosity with more exposed electrochemical sites. A preliminary study was reported by Cao et al. [102], who coated MoS_2 with graphene flakes through chemical vapor deposition (CVD). The authors reported a reversible capacity of 877 mAh g^{-1} that decreased to 53% after 10 cycles at very high current densities of up to 4 A g^{-1}. Chen et al. [103] shifted toward a solvothermal synthesis process, using acid media to induce the nucleation of MoS_2 onto graphene layers. The authors achieved a specific capacity of 1229 mAh g^{-1}, with a decrease to 77% after 50 cycles at 0.1 A g^{-1}. Zhao et al. [104] made further advances, producing an aerogel-like system with a remarkable stability of over 91% at 0.1 A g^{-1} after 25 cycles. Similarly, Wang et al. [105] used a freeze-drying approach to achieve a quasi-totally reversible system with a current density of 0.1 A g^{-1}. Both the production of graphene and its integration into these processes are difficult, but GO and rGO represent a good compromise between feasibility and results. Teng et al. [106] created a GO-based material through simple impregnation, achieving a specific capacity of up to 1077 mAh g^{-1} at 0.1 A g^{-1} and a long cycle lifespan. The authors suggested that the interfacial interaction between oxygen residues and molybdenum atoms enhanced the electron transport rate and structural stability of the MoS_2 hybrid composites. Graphene-rich domains of GO concurrently improved the electrical conductivity and prevented volume changes by being tightly stacked onto MoS_2. Xiong et al. [107] coupled rGO with MoS_2 nanoflowers, obtaining high specific capacity up to 1225 mAh g^{-1} together with an excellent cycling performance of up to 680 mAh g^{-1} after 250 cycles. The authors reported that the 3D network formed was able to improve both the electronic conductivity and strain release during lithiation–delithiation. The crumpled RGO-decorated MoS_2-nanoflower anode exhibits high specific capacity. Similar results were also reported by Li et al. [155] using a similar structure based on rGO, proving that the incorporation of rGO significantly reduces contact resistance. The relevance of the 3D structure on the final performance was also observed for neat graphene-based composites [156].

Modification of graphene can also improve the overall properties, as reported by Wang et al. [109]. The authors combined MoS_2 with graphdiyne oxide to achieve a capacity of 653 mAh g^{-1} at 20 A g^{-1} with nearly perfect reversibility even after 1000 cycles. This was ascribed to the enlargement of the MoS_2 interlayer space, which provided additional Li^+ diffusion channels and storage sites that mitigated the volume changes simultaneously. Additionally, the use of graphdiyne oxide created interfacial electrical fields that improved the Li^+ transport kinetics regulating the interfacial charges distribution during lithiation/delithiation processes. Similar results can be achieved by nitrogen-doping the pristine graphene structure, as reported by Zhao et al. [110] using wet routes, or by using plasma, as discussed by Jiao et al. [111].

Other graphitic carbon materials can be fruitfully used by exploiting their complex 3D geometry to stabilize MoS_2; these include carbon nanosheets [112], mesoporous carbon [157], amorphous carbon [113], carbon microspheres [114,158] or sponges [115], and carbon nanocages [116].

Conductive polymers, such as poly(aniline) [118] or poly(dopamine) [117], provide alternative solutions to pure carbon-based materials. These polymer-based composites can increase the conductivity of the electrode but also act as a flexible matrix that can mitigate volume changes and defectiveness introduced by structural changes in MoS_2. Additionally, they can participate in redox reactions, further boosting the MoS_2 capacity.

4. A Snapshot of Recent and Future Trends in MoS_2-Based 2D Materials for Li-Ion Batteries and Beyond

The unique physicochemical properties of MoS_2, a member of the TMD family, which include a tunable band-gap, an ultrathin layered structure that facilitates Li^+-ion intercalation, a large surface-to-volume ratio, short lithium diffusion paths, and a variety of active sites allowing for a relatively high theoretical capacity, make it particularly attractive for LIB electrodes [159]. However, clearly, issues remain for the practical deployment of MoS_2 in LIBs, mainly involving the significant volume expansion during lithiation/delithiation, and the tendency for nanosheets to restack, which reduces the active surface area and hinders ion transport.

As the drawbacks of conventional liquid electrolytes, such as flammability, leakage, and dendrite formation, limit the widespread diffusion of advanced, high-energy-density LIBs, solid-state lithium batteries (SSLBs) have emerged as a promising alternative. SSLBs replace the liquid electrolyte with a solid-state counterpart, improving safety and thermal stability, and they have great potential for higher energy densities by using lithium metal anodes [160]. In this evolving paradigm, MoS_2 has shown notable promise not only as an anode material itself (as detailed in the previous section), but also as an empowering constituent in combination with other materials (e.g., it enhances structural stability along with the reversible capacity and cyclic durability in a novel two-dimensional architecture of MoS_2 NS@$Li_7P_3S_{11}$ composite superlattice cathode [161]), and even as a component of the solid electrolyte interface. For instance, studies have demonstrated that few-layered MoS_2 nanosheets can serve as effective interfacial layers between solid electrolytes and electrodes, mitigating interfacial resistance and enhancing ionic transport [162]. Additionally, when engineered at the nanoscale, MoS_2 exhibits high mechanical flexibility and good interfacial compatibility with sulfide- and oxide-based solid electrolytes for SSLBs. Results have shown that such hybrid designs can stabilize the lithium interface, suppress dendritic growth, and maintain long-term cycling performance [163].

To address the limitations of pure MoS_2, researchers have developed hybrid nanostructures by combining MoS_2 with conductive and/or structurally robust materials such as graphene, CNTs, conductive polymers, or metal oxides. Amongst the emerging hybrid

systems, researchers recently showed that those incorporating metal oxides (e.g., TiO_2, Fe_2O_3, MoO_3,...) [164–168], transition metal phosphides [169], or MXenes [170] form heterostructures that offer multiple lithium storage mechanisms, such as intercalation and conversion reactions, within a single framework. This multi-modal approach is seen as a path toward achieving both high-capacity and robust cycling performance.

Looking ahead, several advanced strategies are being pursued to further unlock the potential of MoS_2 and similar 2D materials in LIBs:

- Phase engineering: Controlling the ratio of 1T to 2H phases can optimize the balance between conductivity and stability. Methods such as lithium intercalation, chemical doping, or plasma treatment are being used to manipulate the phase composition.
- Defect engineering and doping: Introducing defects or heteroatoms (e.g., N, S, or Se) into the MoS_2 lattice can create additional active sites and modulate the electronic properties to improve performance.
- Scalable and green synthesis: Large-scale production techniques (such as CVD, hydrothermal methods, and electrochemical exfoliation) are being optimized to meet industrial demands while minimizing environmental impacts and production costs.
- Artificial intelligence (AI) and machine-learning-guided optimization: Data-driven approaches are being increasingly employed to predict material properties, screen potential hybrids, and optimize battery performance with minimal trial-and-error experimentation [171].

These critical points can also be addressed though breakthrough approaches, including through the use of advanced artificial intelligence (AI), which can be used to boost the optimization of MoS_2-based LIBs. Specifically, AI can be trained by using the great available dataset, particularly through machine learning algorithms based on large datasets derived from density functional theory (DFT) calculations and experimental data to predict key material properties such as specific capacity, lithium diffusion barriers, structural stability, and electrical conductivity. Even though this research field is still very young, the very same approach was used for optimizing both MoS_2 synthesis [172] and the formulation of the whole electrochemical system (in that case, targeting electrocatalytic processes). Nevertheless, there is still room for improvement in the battery field, as reported by Chen et al. [173] and Kilic. et al. [174].

MoS_2 has also attracted significant attention as a promising electrode material for next-generation batteries beyond LIBs, such as sodium-ion, potassium-ion, and magnesium-ion batteries. Its layered structure, large interlayer spacing, and high theoretical capacity enable efficient ion intercalation and diffusion, even for larger ions like Na^+ and K^+ [175,176]. Moreover, MoS_2 offers good mechanical flexibility and chemical stability, which are essential for sustaining prolonged cycling performance in these systems [177]. Recent studies have demonstrated that engineering MoS_2 nanostructures can further enhance ion-transport kinetics and accommodate volume changes during cycling, making it a versatile candidate for new upcoming energy-storage technologies, including high-energy post-Li batteries and other high-power systems [178,179]. Indeed, both pure MoS_2 and its composites with carbon-based materials, conducting polymers, metal oxides, carbides, and nitrides have been extensively employed in developing novel supercapacitors with significantly enhanced performances, including improved stability and overall capacitance [180]. Particularly for those devices that need the use/integration of flexible/wearable electrodes, MoS_2 and its composites/hybrids show promising prospects due to their high mechanical strength, flexibility, high surface area, and low toxicity [181]. Considering post-lithium energy-storage devices, MoS_2 has also shown potential as an electrode material for Mg-ion batteries owing to its layered structure and relatively wide interlayer spacing, which can facilitate the insertion of divalent Mg^{2+} ions [182]. Although Mg^{2+} ions interact more

strongly with the host material than monovalent ions, resulting in slower diffusion kinetics, strategies such as nanostructuring and defect engineering have been employed to enhance ion mobility and improve electrochemical performance. Recent studies have demonstrated that exfoliated MoS_2 and related composites can deliver promising capacities and cycling stability in Mg-based systems, indicating its versatility for multivalent ion storage [183]. MoS_2 has been already explored as cathode material in Zn-based batteries, which represents a significant area of research interest as a promising alternative technology for large-scale energy storage, primarily due to the cost advantage of zinc over lithium as well as due to the use of conventional aqueous electrolytes, which avoids flammability risks while concurrently providing high ionic mobility [149]. The main challenges in reversibly storing Zn^{2+} in aqueous systems (hydrated zinc ions exhibit relatively large dimensions, necessitating significant energy for intercalation into MoS_2 to break the bond with water molecules) can be mitigated by fine-tuning the structure, particularly by interlayer expansion, while concurrently enhancing the surface/interface hydrophobicity, as demonstrated by Liang et al. [184], who achieved a ten-fold increase in specific capacity (232 mAh g^{-1} at 100 mA g^{-1}), opening up interesting opportunities for its use in aqueous Zn batteries.

5. Conclusions

The surge in energy-storage-related applications by our modern energy-voracious society has accelerated the demand for high-performance LIBs that are not only energy-dense but also safer, longer-lasting, and environmentally sustainable. This, in turn, has heightened the need for promising next-generation candidates as electrodes for high-performance LIBs. Within this framework, two-dimensional (2D) materials stand out as transformative candidates for use both in high-energy and high-power-density devices due to their unique physicochemical properties, including their layered structure that facilitates Li^+ ion intercalation, a tunable band-gap, and a relatively high theoretical capacity.

Molybdenum disulfide (MoS_2), a member of the TMD family, consists of layers bonded by weak Van der Waals forces, which allows for its easy exfoliation into atomically thin nanosheets. These ultrathin layers offer a large surface-to-volume ratio, short lithium diffusion paths, and a variety of active sites, making it particularly attractive for LIB electrodes. The two primary crystalline phases, semiconducting 2H and metallic 1T, present different electronic and electrochemical characteristics. While the 2H phase is more stable, the 1T phase offers superior conductivity, which can be beneficial for enhancing rate performance. The high capacity and layered structure of MoS_2 are complemented by the excellent conductivity, flexibility, and mechanical stability of the secondary phase (s), allowing for enhanced specific capacities (often >1000 mAh g^{-1}), excellent rate capabilities, and long-term cycling stability by maintaining a high surface area and accessibility of active sites and resisting volumetric strain during charge/discharge cycles.

Despite its promising electrochemical properties, several inherent limitations and key challenges must be addressed for MoS_2 prior to its widespread use in commercial battery applications. Chiefly, these include poor intrinsic electrical conductivity, significant volume expansion during lithiation/delithiation, and a tendency for nanosheets to restack, which reduce the active surface area and hinder ion transport. These main issues, such as poor conductivity and fragility, can be solved by combining MoS_2 together with carbon-based materials or inorganic species with synergistic effects that boost the conductivity and reduce structural instability during repeated charge/discharge cycling. Industrial exploitation can be achieved only by enhancing the scalability of its synthesis processes, which are often costly, energy-intensive, and difficult to control at large volumes. Moreover, maintaining consistent material quality, such as uniform morphology and phase purity, is critical and particularly challenging during large-scale production. The mechanical

instability of MoS_2 during long-term cycling, leading to electrode pulverization, also poses a serious barrier to meeting industrial durability standards. Finally, integrating MoS_2 into existing manufacturing lines without significantly increasing costs or complicating electrode fabrication processes remains a major hurdle.

The integration of MoS_2 and other 2D materials into LIBs, particularly in solid-state and hybrid configurations, represents a rapidly advancing frontier with the potential to dramatically enhance battery performance. Continuous progress will depend on a deep understanding of electrochemical mechanisms at the atomic level, as well as on the development of scalable fabrication techniques and stable material combinations. By bridging fundamental materials science with practical engineering, MoS_2-based batteries are poised to play a pivotal role in the future of energy-storage technology.

Author Contributions: Conceptualization, M.B., G.A.E., C.G., G.M. and A.P.; investigation, M.B., M.B.C., Ö.D.C., S.P., D.P., E.P., F.G., G.A.E., C.G., G.M. and A.P.; resources, C.G.; data curation, M.B., M.B.C., Ö.D.C., S.P., D.P., E.P., F.G., G.A.E., C.G., G.M. and A.P.; writing—original draft preparation, review and editing M.B., M.B.C., Ö.D.C., S.P., D.P., E.P., F.G., G.A.E., C.G., G.M. and A.P. writing—review and editing, M.B., M.B.C., Ö.D.C., S.P., D.P., E.P., F.G., G.A.E., C.G., G.M. and A.P.; visualization, M.B.; supervision, G.A.E., C.G. and A.P.; project administration, G.A.E., C.G. and A.P.; funding acquisition, G.A.E., C.G. and A.P. All authors have read and agreed to the published version of the manuscript.

Funding: This study was carried out within the MOST–Sustainable Mobility Center and received funding from the European Union Next–Generation EU (PIANO NAZIONALE DI RIPRESA E RESILIENZA–PNRR–MISSIONE 4 COMPONENTE 2, INVESTIMENTO 1.4 e D.D. 1033 17 June 2022, CN00000023); within the EnabLi project, funded by the Ministero dell'Università e della Ricerca; and within the PRIN 2022-1208/2023 (program D.D.104-02/02/2022). This manuscript reflects only the authors' views and opinions; neither the European Union nor the European Commission can be considered responsible for them. M.B., E.P., S.P., A.P., G.A.E., and C.G. acknowledge support under the MUR program Dipartimenti di Eccellenza 2023–2027 (CUPE17G22001490006). The authors acknowledge the program Piano Triennale della Ricerca (PTR) within the Ricerca Sistema Elettrico Nazionale 2025–2027, funded through contributions to research and development by the Italian Ministry of Economic Development. M.B.C. and Ö.D.C. thank the Hacettepe University Scientific Research Coordination Unit for the research grant under project number FUI-2022-20288. D.P. acknowledges the support from the European Union—NextGenerationEU under the National Recovery and Resilience Plan (NRRP), Mission 04 Component 2 Investment 3.1 | Project Code: IR0000027—CUP: B33C22000710006—iENTRANCE@ENL: Infrastructure for Energy TRAnsition aNd Circular Economy @EuroNanoLab. E.P. acknowledges funding by the European Union–Next Generation EU as part of the PRIN 2022 PNRR project "Continuous THERmal monitoring with wearable mid-InfraRed sensors" (P2022AHXE5).

Conflicts of Interest: The authors declare no conflicts of interest.

References

1. Ajayan, P.; Kim, P.; Banerjee, K. Two-dimensional van der Waals materials. *Phys. Today* **2016**, *69*, 38–44. [CrossRef]
2. Marian, M.; Berman, D.; Rota, A.; Jackson, R.L.; Rosenkranz, A. Layered 2D nanomaterials to tailor friction and wear in machine elements—A review. *Adv. Mater. Interfaces* **2022**, *9*, 2101622. [CrossRef]
3. Castro Neto, A.H.; Guinea, F.; Peres, N.M.R.; Novoselov, K.S.; Geim, A.K. The electronic properties of graphene. *Rev. Mod. Phys.* **2009**, *81*, 109–162. [CrossRef]
4. Jariwala, D.; Sangwan, V.K.; Lauhon, L.J.; Marks, T.J.; Hersam, M.C. Carbon nanomaterials for electronics, optoelectronics, photovoltaics, and sensing. *Chem. Soc. Rev.* **2013**, *42*, 2824–2860. [CrossRef] [PubMed]
5. Mannix, A.J.; Kiraly, B.; Hersam, M.C.; Guisinger, N.P. Synthesis and chemistry of elemental 2D materials. *Nat. Rev. Chem.* **2017**, *1*, 0014. [CrossRef]
6. Choi, S.H.; Yun, S.J.; Won, Y.S.; Oh, C.S.; Kim, S.M.; Kim, K.K.; Lee, Y.H. Large-scale synthesis of graphene and other 2D materials towards industrialization. *Nat. Commun.* **2022**, *13*, 1484. [CrossRef] [PubMed]

7. Kozhakhmetov, A.; Torsi, R.; Chen, C.Y.; Robinson, J.A. Scalable low-temperature synthesis of two-dimensional materials beyond graphene. *J. Phys. Mater.* **2020**, *4*, 012001. [CrossRef]
8. Alli, U.; Hettiarachchi, S.J.; Kellici, S. Chemical functionalisation of 2D materials by batch and continuous hydrothermal flow synthesis. *Chem. A Eur. J.* **2020**, *26*, 6447–6460. [CrossRef] [PubMed]
9. Mazzotta, S.; Lettieri, S.; Ferraro, G.; Bartoli, M.; Etzi, M.; Pirri, C.F.; Bocchini, S. A Concise Overview of Ultrasound-Assisted Techniques for the Production of 2D Materials. *Processes* **2024**, *12*, 759. [CrossRef]
10. Zago, S.; Bartoli, M.; Muhyuddin, M.; Vanacore, G.M.; Jagdale, P.; Tagliaferro, A.; Santoro, C.; Specchia, S. Engineered biochar derived from pyrolyzed waste tea as a carbon support for Fe-N-C electrocatalysts for the oxygen reduction reaction. *Electrochim. Acta* **2022**, *412*, 140128. [CrossRef]
11. Yu, J.; Hu, X.; Li, H.; Zhou, X.; Zhai, T. Large-scale synthesis of 2D metal dichalcogenides. *J. Mater. Chem. C* **2018**, *6*, 4627–4640. [CrossRef]
12. Dean, C.R.; Young, A.F.; Meric, I.; Lee, C.; Wang, L.; Sorgenfrei, S.; Watanabe, K.; Taniguchi, T.; Kim, P.; Shepard, K.L.; et al. Boron nitride substrates for high-quality graphene electronics. *Nat. Nanotechnol.* **2010**, *5*, 722–726. [CrossRef] [PubMed]
13. Wang, Q.H.; Kalantar-Zadeh, K.; Kis, A.; Coleman, J.N.; Strano, M.S. Electronics and optoelectronics of two-dimensional transition metal dichalcogenides. *Nat. Nanotechnol.* **2012**, *7*, 699–712. [CrossRef] [PubMed]
14. Butler, S.Z.; Hollen, S.M.; Cao, L.; Cui, Y.; Gupta, J.A.; Gutiérrez, H.R.; Heinz, T.F.; Hong, S.S.; Huang, J.; Ismach, A.F.; et al. Progress, challenges, and opportunities in two-dimensional materials beyond graphene. *ACS Nano* **2013**, *7*, 2898–2926. [CrossRef] [PubMed]
15. Wilson, J.A.; Yoffe, A. The transition metal dichalcogenides discussion and interpretation of the observed optical, electrical and structural properties. *Adv. Phys.* **1969**, *18*, 193–335. [CrossRef]
16. Bandurin, D.A.; Tyurnina, A.V.; Yu, G.L.; Mishchenko, A.; Zólyomi, V.; Morozov, S.V.; Kumar, R.K.; Gorbachev, R.V.; Kudrynskyi, Z.R.; Pezzini, S.; et al. High electron mobility, quantum Hall effect and anomalous optical response in atomically thin InSe. *Nat. Nanotechnol.* **2017**, *12*, 223–227. [CrossRef] [PubMed]
17. Wang, F.K.; Yang, S.J.; Zhai, T.Y. 2D Bi2Se3 materials for optoelectronics. *Iscience* **2021**, *24*, 103291. [CrossRef] [PubMed]
18. Naguib, M.; Mochalin, V.N.; Barsoum, M.W.; Gogotsi, Y. 25th anniversary article: MXenes: A new family of two-dimensional materials. *Adv. Mater.* **2014**, *26*, 992–1005. [CrossRef] [PubMed]
19. Thomas, J.; Jezequel, G.; Pollini, I. Optical properties of layered transition-metal halides. *J. Phys. Condens. Matter* **1990**, *2*, 5439. [CrossRef]
20. McGuire, M.A.; Dixit, H.; Cooper, V.R.; Sales, B.C. Coupling of crystal structure and magnetism in the layered, ferromagnetic insulator CrI3. *Chem. Mater.* **2015**, *27*, 612–620. [CrossRef]
21. Ma, R.; Sasaki, T. Two-dimensional oxide and hydroxide nanosheets: Controllable high-quality exfoliation, molecular assembly, and exploration of functionality. *Accounts Chem. Res.* **2015**, *48*, 136–143. [CrossRef] [PubMed]
22. Cao, D.H.; Stoumpos, C.C.; Farha, O.K.; Hupp, J.T.; Kanatzidis, M.G. 2D homologous perovskites as light-absorbing materials for solar cell applications. *J. Am. Chem. Soc.* **2015**, *137*, 7843–7850. [CrossRef] [PubMed]
23. Tao, L.; Cinquanta, E.; Chiappe, D.; Grazianetti, C.; Fanciulli, M.; Dubey, M.; Molle, A.; Akinwande, D. Silicene field-effect transistors operating at room temperature. *Nat. Nanotechnol.* **2015**, *10*, 227–231. [CrossRef] [PubMed]
24. Ling, X.; Wang, H.; Huang, S.; Xia, F.; Dresselhaus, M.S. The renaissance of black phosphorus. *Proc. Natl. Acad. Sci. USA* **2015**, *112*, 4523–4530. [CrossRef] [PubMed]
25. Zhang, Y.; Zhang, R.; Guo, Y.; Li, Y.; Li, K. A review on MoS_2 structure, preparation, energy storage applications and challenges. *J. Alloys Compd.* **2024**, *998*, 174916. [CrossRef]
26. Yadav, A.; Sharma, A.K.; Yadav, J.; Bhasker, S.; Mishra, G.; Bhasker, H.P.; Patel, S.P.; Dhawan, P.K.; Chaudhary, D.K. Morphological impact on energy storage properties of 2D-MoS_2 and its nanocomposites: A comprehensive review. *Z. Naturforsch. A* **2025**, *80*, 345–362. [CrossRef]
27. Sangwan, V.K.; Hersam, M.C. Electronic transport in two-dimensional materials. *Annu. Rev. Phys. Chem.* **2018**, *69*, 299–325. [CrossRef] [PubMed]
28. Bergeron, H.; Lebedev, D.; Hersam, M.C. Polymorphism in post-dichalcogenide two-dimensional materials. *Chem. Rev.* **2021**, *121*, 2713–2775. [CrossRef] [PubMed]
29. Molaei, M.J.; Younas, M.; Rezakazemi, M. A comprehensive review on recent advances in two-dimensional (2D) hexagonal boron nitride. *ACS Appl. Electron. Mater.* **2021**, *3*, 5165–5187. [CrossRef]
30. Fan, F.R.; Wang, R.; Zhang, H.; Wu, W. Emerging beyond-graphene elemental 2D materials for energy and catalysis applications. *Chem. Soc. Rev.* **2021**, *50*, 10983–11031. [CrossRef] [PubMed]
31. Tang, W.; Yu, K.; Zhou, Z.; Li, J.; Gao, L. Preparation of two-dimensional superconductors: A comprehensive review. *J. Mater. Chem. C* **2025**, *13*, 6963–6979. [CrossRef]
32. Fiori, G.; Bonaccorso, F.; Iannaccone, G.; Palacios, T.; Neumaier, D.; Seabaugh, A.; Banerjee, S.K.; Colombo, L. Electronics based on two-dimensional materials. *Nat. Nanotechnol.* **2014**, *9*, 768–779. [CrossRef] [PubMed]

33. Tedstone, A.A.; Lewis, D.J.; Hao, R.; Mao, S.-M.; Bellon, P.; Averback, R.S.; Warrens, C.P.; West, K.R.; Howard, P.; Gaemers, S.; et al. Mechanical Properties of Molybdenum Disulfide and the Effect of Doping: An in Situ TEM Study. *ACS Appl. Mater. Interfaces* **2015**, *7*, 20829–20834. [CrossRef] [PubMed]
34. Li, X.; Zhu, H. Two-dimensional MoS2: Properties, preparation, and applications. *J. Materiomics* **2015**, *1*, 33–44. [CrossRef]
35. Ghorbani-Asl, M.; Zibouche, N.; Wahiduzzaman, M.; Oliveira, A.F.; Kuc, A.; Heine, T. Electromechanics in MoS_2 and WS_2: Nanotubes vs. monolayers. *Sci. Rep.* **2013**, *3*, 2961. [CrossRef] [PubMed]
36. Bertolazzi, S.; Brivio, J.; Kis, A. Stretching and Breaking of Ultrathin MoS_2. *ACS Nano* **2011**, *5*, 9703–9709. [CrossRef] [PubMed]
37. Castellanos-Gomez, A.; Poot, M.; Steele, G.A.; van der Zant, H.S.J.; Agraït, N.; Rubio-Bollinger, G. Elastic Properties of Freely Suspended MoS_2 Nanosheets. *Adv. Mater.* **2012**, *24*, 772–775. [CrossRef] [PubMed]
38. Halim, S.N.M.; Zuikafly, S.N.F.; Taib, M.F.M.; Ahmad, F. First Principles Study on Electronic and Optical Properties of Graphene/MoS_2 for Optoelectronic Application. In Proceedings of the 2020 IEEE International Conference on Semiconductor Electronics (ICSE), Kuala Lumpur, Malaysia, 28–29 July 2020; pp. 29–32.
39. Nalwa, H.S. A review of molybdenum disulfide (MoS_2) based photodetectors: From ultra-broadband, self-powered to flexible devices. *RSC Adv.* **2020**, *10*, 30529–30602. [CrossRef] [PubMed]
40. Cheng, Y.; Wang, J.-Z.; Wei, X.-X.; Guo, D.; Wu, B.; Yu, L.-W.; Wang, X.-R.; Shi, Y. Tuning Photoluminescence Performance of Monolayer MoS_2 via H_2O_2 Aqueous Solution*. *Chin. Phys. Lett.* **2015**, *32*, 117801. [CrossRef]
41. Johari, P.; Shenoy, V.B. Tuning the Electronic Properties of Semiconducting Transition Metal Dichalcogenides by Applying Mechanical Strains. *ACS Nano* **2012**, *6*, 5449–5456. [CrossRef] [PubMed]
42. Kadantsev, E.S.; Hawrylak, P. Electronic structure of a single MoS_2 monolayer. *Solid State Commun.* **2012**, *152*, 909–913. [CrossRef]
43. Tsai, Y.C.; Li, Y. Impact of Doping Concentration on Electronic Properties of Transition Metal-Doped Monolayer Molybdenum Disulfide. *IEEE Trans. Electron Devices* **2018**, *65*, 733–738. [CrossRef]
44. Liu, H.; Huang, Z.; Qiao, H.; Qi, X. Characteristics and performance of layered two-dimensional materials under doping engineering. *Phys. Chem. Chem. Phys.* **2024**, *26*, 17423–17442. [CrossRef] [PubMed]
45. Cui, Z.; Li, M.; Li, E.; Ma, D.; Zhao, B. First-principles study of antimony-doped monolayer molybdenum disulfide: Electronic structure and optical properties. *Phys. E Low-Dimens. Syst. Nanostruct.* **2018**, *104*, 91–97. [CrossRef]
46. Wang, Q.; Wang, X.; Huang, S.; Zhang, Y.; Chen, Z. Integrated design of sandwich-like C@MoS_2@C nanospheres as active anode material for lithium-ion batteries. *J. Mater. Sci.* **2022**, *57*, 14948–14958. [CrossRef]
47. Zhang, H.; Song, J.; Li, J.; Feng, J.; Ma, Y.; Ma, L.; Liu, H.; Qin, Y.; Zhao, X.; Wang, F. Interlayer-expanded MoS_2 nanoflowers vertically aligned on MXene@dual-phased TiO_2 as high-performance anode for sodium-ion batteries. *ACS Appl. Mater. Interfaces* **2022**, *14*, 16300–16309. [CrossRef] [PubMed]
48. Guguchia, Z.; Kerelsky, A.; Edelberg, D.; Banerjee, S.; von Rohr, F.; Scullion, D.; Augustin, M.; Scully, M.; Rhodes, D.A.; Shermadini, Z.; et al. Magnetism in semiconducting molybdenum dichalcogenides. *Sci. Adv.* **2018**, *4*, eaat3672. [CrossRef] [PubMed]
49. Tongay, S.; Varnoosfaderani, S.S.; Appleton, B.R.; Wu, J.; Hebard, A.F. Magnetic properties of MoS_2: Existence of ferromagnetism. *Appl. Phys. Lett.* **2012**, *101*, 123105. [CrossRef]
50. Liang, S.; Yang, H.; Renucci, P.; Tao, B.; Laczkowski, P.; Mc-Murtry, S.; Wang, G.; Marie, X.; George, J.-M.; Petit-Watelot, S.; et al. Electrical spin injection and detection in molybdenum disulfide multilayer channel. *Nat. Commun.* **2017**, *8*, 14947. [CrossRef] [PubMed]
51. Zhang, G.; Liu, H.; Qu, J.; Li, J. Two-dimensional layered MoS_2: Rational design, properties and electrochemical applications. *Energy Environ. Sci.* **2016**, *9*, 1190–1209. [CrossRef]
52. Wilson, J.A.; Di Salvo, F.; Mahajan, S. Charge-density waves and superlattices in the metallic layered transition metal dichalcogenides. *Adv. Phys.* **1975**, *24*, 117–201. [CrossRef]
53. Xu, M.; Liang, T.; Shi, M.; Chen, H. Graphene-like two-dimensional materials. *Chem. Rev.* **2013**, *113*, 3766–3798. [CrossRef] [PubMed]
54. Piatti, E.; Prando, G.; Meinero, M.; Tresca, C.; Putti, M.; Roddaro, S.; Lamura, G.; Shiroka, T.; Carretta, P.; Profeta, G.; et al. Superconductivity induced by gate-driven hydrogen intercalation in the charge-density-wave compound 1T-$TiSe_2$. *Commun. Phys.* **2023**, *6*, 202. [CrossRef]
55. Mak, K.F.; Lee, C.; Hone, J.; Shan, J.; Heinz, T.F. Atomically thin MoS_2: A new direct-gap semiconductor. *Phys. Rev. Lett.* **2010**, *105*, 136805. [CrossRef] [PubMed]
56. Piatti, E.; Galasso, S.; Tortello, M.; Nair, J.; Gerbaldi, C.; Bruna, M.; Borini, S.; Daghero, D.; Gonnelli, R. Carrier mobility and scattering lifetime in electric double-layer gated few-layer graphene. *Appl. Surf. Sci.* **2017**, *395*, 37–41. [CrossRef]
57. Romanin, D.; Brumme, T.; Daghero, D.; Gonnelli, R.S.; Piatti, E. Strong band-filling-dependence of the scattering lifetime in gated MoS_2 nanolayers induced by the opening of intervalley scattering channels. *J. Appl. Phys.* **2020**, *128*, 063907. [CrossRef]
58. Narita, S.-I.; Terada, S.-I.; Mori, S.; Muro, K.; Akahama, Y.; Endo, S. Far-infrared cyclotron resonance absorptions in black phosphorus single crystals. *J. Phys. Soc. Jpn.* **1983**, *52*, 3544–3553. [CrossRef]

59. Allain, A.; Kang, J.; Banerjee, K.; Kis, A. Electrical contacts to two-dimensional semiconductors. *Nat. Mater.* **2015**, *14*, 1195–1205. [CrossRef] [PubMed]
60. Wang, L.; Meric, I.; Huang, P.Y.; Gao, Q.; Gao, Y.; Tran, H.; Taniguchi, T.; Watanabe, K.; Campos, L.M.; Muller, D.A.; et al. One-dimensional electrical contact to a two-dimensional material. *Science* **2013**, *342*, 614–617. [CrossRef] [PubMed]
61. Piatti, E.; Arbab, A.; Galanti, F.; Carey, T.; Anzi, L.; Spurling, D.; Roy, A.; Zhussupbekova, A.; Patel, K.A.; Kim, J.M.; et al. Charge transport mechanisms in inkjet-printed thin-film transistors based on two-dimensional materials. *Nat. Electron.* **2021**, *4*, 893–905. [CrossRef]
62. Zheng, W.; Sun, B.; Li, D.; Gali, S.M.; Zhang, H.; Fu, S.; Di Virgilio, L.; Li, Z.; Yang, S.; Zhou, S.; et al. Band transport by large Fröhlich polarons in MXenes. *Nat. Phys.* **2022**, *18*, 544–550. [CrossRef]
63. Haering, R.R.; Stiles, J.A.; Brandt, K. Lithium Molybdenum Disulphide Battery Cathode. U.S. Patent US4224390A, 23 September 1980.
64. Samy, O.; El Moutaouakil, A. A review on MoS_2 energy applications: Recent developments and challenges. *Energies* **2021**, *14*, 4586. [CrossRef]
65. Cordeiro, N.J.A.; Gaspar, C.; de Oliveira, M.J.; Nunes, D.; Barquinha, P.; Pereira, L.; Fortunato, E.; Martins, R.; Laureto, E.; Lourenço, S.A. Fast and low-cost synthesis of MoS_2 nanostructures on paper substrates for near-infrared photodetectors. *Appl. Sci.* **2021**, *11*, 1234. [CrossRef]
66. Tao, R.; Gu, Y.; Du, Z.; Lyu, X.; Li, J. Advanced electrode processing for lithium-ion battery manufacturing. *Nat. Rev. Clean Technol.* **2025**, *1*, 116–131. [CrossRef]
67. Fang, X.; Hua, C.; Guo, X.; Hu, Y.; Wang, Z.; Gao, X.; Wu, F.; Wang, J.; Chen, L. Lithium storage in commercial MoS_2 in different potential ranges. *Electrochim. Acta* **2012**, *81*, 155–160. [CrossRef]
68. Bissett, M.A.; Kinloch, I.A.; Dryfe, R.A. Characterization of MoS_2–graphene composites for high-performance coin cell supercapacitors. *ACS Appl. Mater. Interfaces* **2015**, *7*, 17388–17398. [CrossRef] [PubMed]
69. Li, Z.; Yang, Z.J.; Moloney, J.; Yu, C.P.; Chhowalla, M. Quasi-solid-state electrolyte induced by metallic MoS_2 for lithium–sulfur batteries. *ACS Nano* **2024**, *18*, 16041–16050. [CrossRef] [PubMed]
70. Lv, X.; Guo, W.; Song, J.; Fu, Y. Dynamic 1T-2H Mixed-Phase MoS_2 Enables High-Performance Li-Organosulfide Battery. *Small* **2022**, *18*, 2105071. [CrossRef] [PubMed]
71. Lei, Y.; Chen, M.; Li, Y.; Zhang, W.; Zhao, D.; Zhu, Q. Dendrite-free potassium metal anode induced by in-situ phase transitions of MoS_2. *Mater. Today Phys.* **2023**, *35*, 101141. [CrossRef]
72. Wang, W.; Zhang, W.; Yu, R.; Qiao, F.; Wang, J.; Wang, J.; An, Q. Molecular Engineering to Construct MoS_2 with Expanded Interlayer Spacing and Enriched 1T Phase for "Rocking-Chair" Aqueous Calcium-Ion Pouch Cells. *ACS Nano* **2024**, *18*, 35286–35295. [CrossRef] [PubMed]
73. Feng, C.; Ma, J.; Li, H.; Zeng, R.; Guo, Z.; Liu, H. Synthesis of molybdenum disulfide (MoS_2) for lithium ion battery applications. *Mater. Res. Bull.* **2009**, *44*, 1811–1815. [CrossRef]
74. Stephenson, T.; Li, Z.; Olsen, B.; Mitlin, D. Lithium ion battery applications of molybdenum disulfide (MoS_2) nanocomposites. *Energy Environ. Sci.* **2014**, *7*, 209–231. [CrossRef]
75. Miki, Y.; Nakazato, D.; Ikuta, H.; Uchida, T.; Wakihara, M. Amorphous MoS_2 as the cathode of lithium secondary batteries. *J. Power Sources* **1995**, *54*, 508–510. [CrossRef]
76. Jiao, Y.; Hafez, A.M.; Cao, D.; Mukhopadhyay, A.; Ma, Y.; Zhu, H. Metallic MoS_2 for high performance energy storage and energy conversion. *Small* **2018**, *14*, 1800640. [CrossRef] [PubMed]
77. Han, M.; Mu, Y.; Guo, J.; Wei, L.; Zeng, L.; Zhao, T. Monolayer MoS_2 Fabricated by In Situ Construction of Interlayer Electrostatic Repulsion Enables Ultrafast Ion Transport in Lithium-Ion Batteries. *Nano-Micro Lett.* **2023**, *15*, 80. [CrossRef] [PubMed]
78. Wu, Z.; Li, B.; Xue, Y.; Li, J.; Zhang, Y.; Gao, F. Fabrication of defect-rich MoS_2 ultrathin nanosheets for application in lithium-ion batteries and supercapacitors. *J. Mater. Chem. A* **2015**, *3*, 19445–19454. [CrossRef]
79. Liu, Y.; Zhang, L.; Zhao, Y.; Shen, T.; Yan, X.; Yu, C.; Wang, H.; Zeng, H. Novel plasma-engineered MoS_2 nanosheets for superior lithium-ion batteries. *J. Alloys Compd.* **2019**, *787*, 996–1003. [CrossRef]
80. Liu, Q.; Xia, W.; Wu, Z.; Huo, J.; Liu, D.; Wang, Q.; Wang, S. The origin of the enhanced performance of nitrogen-doped MoS_2 in lithium ion batteries. *Nanotechnology* **2016**, *27*, 175402. [CrossRef] [PubMed]
81. Sun, C.; Zhao, K.; He, Y.; Zheng, J.; Xu, W.; Zhang, C.; Wang, X.; Guo, M.; Mai, L.; Wang, C.; et al. Interconnected Vertically Stacked 2D-MoS_2 for Ultrastable Cycling of Rechargeable Li-Ion Battery. *ACS Appl. Mater. Interfaces* **2019**, *11*, 20762–20769. [CrossRef] [PubMed]
82. Park, J.; Bhoyate, S.; Kim, Y.-H.; Kim, Y.-M.; Lee, Y.H.; Conlin, P.; Cho, K.; Choi, W. Unusually high ion conductivity in large-scale patternable two-dimensional MoS_2 film. *ACS Nano* **2021**, *15*, 12267–12275. [CrossRef] [PubMed]
83. Venkateshwaran, S.; Partheeban, T.; Sasidharan, M.; Senthil Kumar, S.M. Mesoporous Silica Template-Assisted Synthesis of 1T-MoS_2 as the Anode for Li-Ion Battery Applications. *Energy Fuels* **2021**, *35*, 2683–2691. [CrossRef]
84. Wang, P.-P.; Sun, H.; Ji, Y.; Li, W.; Wang, X. Three-Dimensional Assembly of Single-Layered MoS_2. *Adv. Mater.* **2014**, *26*, 964–969. [CrossRef] [PubMed]

85. Zhao, X.; Liu, Z.; Xiao, W.; Huang, H.; Zhang, L.; Cheng, Y.; Zhang, J. Low Crystalline MoS_2 Nanotubes from MoS_2 Nanomasks for Lithium Ion Battery Applications. *ACS Appl. Nano Mater.* **2020**, *3*, 7580–7586. [CrossRef]
86. Faizan, M.; Hussain, S.; Islam, M.; Kim, J.-Y.; Han, D.; Bae, J.-H.; Vikraman, D.; Ali, B.; Abbas, S.; Kim, H.-S.; et al. MoO_3@MoS_2 Core-Shell Structured Hybrid Anode Materials for Lithium-Ion Batteries. *Nanomaterials* **2022**, *12*, 2008. [CrossRef] [PubMed]
87. Zhao, C.; Fu, J.; Shen, A.; Zhang, L.; Kong, S.; Feng, Y.; Gong, W.; Tian, K.; Li, Q. Interfacial coupling of MoS_2/MoO_3 hierarchical heterostructures as superior anodes for high-performance lithium-ion battery. *J. Energy Storage* **2023**, *72*, 108595. [CrossRef]
88. Lei, D.; Shang, W.; Zhang, X.; Li, Y.; Qiao, S.; Zhong, Y.; Deng, X.; Shi, X.; Zhang, Q.; Hao, C. Facile synthesis of heterostructured MoS_2–MoO_3 nanosheets with active electrocatalytic sites for high-performance lithium–sulfur batteries. *ACS Nano* **2021**, *15*, 20478–20488. [CrossRef] [PubMed]
89. Zhao, S.; Zha, Z.; Liu, X.; Tian, H.; Wu, Z.; Li, W.; Sun, L.-B.; Liu, B.; Chen, Z. Core–sheath structured MoO_3@MoS_2 composite for high-performance lithium-ion battery anodes. *Energy Fuels* **2020**, *34*, 11498–11507. [CrossRef]
90. Zhao, Y.; Wang, W.; Chen, M.; Wang, R.; Fang, Z. The synthesis of ZnS@MoS_2 hollow polyhedrons for enhanced lithium storage performance. *CrystEngComm* **2018**, *20*, 7266–7274. [CrossRef]
91. Zhu, X.; Yang, C.; Xiao, F.; Wang, J.; Su, X. Synthesis of nano-TiO_2-decorated MoS_2 nanosheets for lithium-ion batteries. *New J. Chem.* **2015**, *39*, 683–688. [CrossRef]
92. Xu, W.; Wang, T.; Yu, Y.; Wang, S. Synthesis of core-shell TiO_2@MoS_2 composites for lithium-ion battery anodes. *J. Alloys Compd.* **2016**, *689*, 460–467. [CrossRef]
93. Chen, Z.; Yin, D.; Zhang, M. Sandwich-like MoS_2@SnO_2@C with High Capacity and Stability for Sodium/Potassium Ion Batteries. *Small* **2018**, *14*, e1703818. [CrossRef] [PubMed]
94. Wang, H.; Pan, Q.; Chen, J.; Zan, Y.; Huang, Y.; Yang, G.; Yan, Z.; Li, Q. Facile synthesis of Sn/MoS_2/C composite as an anode material for lithium-ion batteries with outstanding performance. *New J. Chem.* **2016**, *40*, 1263–1268. [CrossRef]
95. Ette, P.M.; Chithambararaj, A.; Prakash, A.S.; Ramesha, K. MoS_2 Nanoflower-Derived Interconnected $CoMoO_4$ Nanoarchitectures as a Stable and High Rate Performing Anode for Lithium-Ion Battery Applications. *ACS Appl. Mater. Interfaces* **2020**, *12*, 11511–11521. [CrossRef] [PubMed]
96. Wang, J.; Zhou, H.; Zhu, M.; Yuan, A.; Shen, X. Metal-organic framework-derived Co_3O_4 covered by MoS_2 nanosheets for high-performance lithium-ion batteries. *J. Alloys Compd.* **2018**, *744*, 220–227. [CrossRef]
97. Samad, A.; Shin, Y.-H. MoS_2@VS_2 Nanocomposite as a Superior Hybrid Anode Material. *ACS Appl. Mater. Interfaces* **2017**, *9*, 29942–29949. [CrossRef] [PubMed]
98. Bindumadhavan, K.; Srivastava, S.K.; Mahanty, S. MoS_2–MWCNT hybrids as a superior anode in lithium-ion batteries. *Chem. Commun.* **2013**, *49*, 1823–1825. [CrossRef] [PubMed]
99. Wang, J.-Z.; Lu, L.; Lotya, M.; Coleman, J.N.; Chou, S.-L.; Liu, H.-K.; Minett, A.I.; Chen, J. Development of MoS_2–CNT composite thin film from layered MoS_2 for lithium batteries. *Adv. Energy Mater.* **2013**, *3*, 798–805. [CrossRef]
100. Yoo, H.; Tiwari, A.P.; Lee, J.; Kim, D.; Park, J.H.; Lee, H. Cylindrical nanostructured MoS_2 directly grown on CNT composites for lithium-ion batteries. *Nanoscale* **2015**, *7*, 3404–3409. [CrossRef] [PubMed]
101. Wang, S.; Guan, B.Y.; Yu, L.; Lou, X.W. Rational Design of Three-Layered TiO_2@Carbon@MoS_2 Hierarchical Nanotubes for Enhanced Lithium Storage. *Adv. Mater.* **2017**, *29*, 1702724. [CrossRef] [PubMed]
102. Cao, X.; Shi, Y.; Shi, W.; Rui, X.; Yan, Q.; Kong, J.; Zhang, H. Preparation of MoS_2-Coated Three-Dimensional Graphene Networks for High-Performance Anode Material in Lithium-Ion Batteries. *Small* **2013**, *9*, 3433–3438. [CrossRef] [PubMed]
103. Chen, L.; Yang, Y.; Gao, Y.; Tronganh, N.; Chen, F.; Lu, M.; Jiang, Y.; Jiao, Z.; Zhao, B. Facile synthesis of ultrathin, undersized MoS_2/graphene for lithium-ion battery anodes. *RSC Adv.* **2016**, *6*, 99833–99841. [CrossRef]
104. Zhao, B.; Wang, Z.; Gao, Y.; Chen, L.; Lu, M.; Jiao, Z.; Jiang, Y.; Ding, Y.; Cheng, L. Hydrothermal synthesis of layer-controlled MoS2/graphene composite aerogels for lithium-ion battery anode materials. *Appl. Surf. Sci.* **2016**, *390*, 209–215. [CrossRef]
105. Wang, S.; Wang, R.; Zhao, Q.; Ren, L.; Wen, J.; Chang, J.; Fang, X.; Hu, N.; Xu, C. Freeze-drying induced self-assembly approach for scalable constructing MoS_2/graphene hybrid aerogels for lithium-ion batteries. *J. Colloid Interface Sci.* **2019**, *544*, 37–45. [CrossRef] [PubMed]
106. Teng, Y.; Zhao, H.; Zhang, Z.; Li, Z.; Xia, Q.; Zhang, Y.; Zhao, L.; Du, X.; Du, Z.; Lv, P.; et al. MoS_2 Nanosheets Vertically Grown on Graphene Sheets for Lithium-Ion Battery Anodes. *ACS Nano* **2016**, *10*, 8526–8535. [CrossRef] [PubMed]
107. Xiong, F.; Cai, Z.; Qu, L.; Zhang, P.; Yuan, Z.; Asare, O.K.; Xu, W.; Lin, C.; Mai, L. Three-Dimensional Crumpled Reduced Graphene Oxide/MoS_2 Nanoflowers: A Stable Anode for Lithium-Ion Batteries. *ACS Appl. Mater. Interfaces* **2015**, *7*, 12625–12630. [CrossRef] [PubMed]
108. Li, H.; Yu, K.; Fu, H.; Guo, B.; Lei, X.; Zhu, Z. MoS_2/Graphene Hybrid Nanoflowers with Enhanced Electrochemical Performances as Anode for Lithium-Ion Batteries. *J. Phys. Chem. C* **2015**, *119*, 7959–7968. [CrossRef]
109. Wang, T.; Li, M.; Qi, L.; Jie, P.; Yang, W.; Li, Y. Multilevel Heterostructure of MoS_2/GDYO for Lithium-Ion Batteries. *Adv. Funct. Mater.* **2023**, *33*, 2308470. [CrossRef]

110. Zhao, C.; Wang, X.; Kong, J.; Ang, J.M.; Lee, P.S.; Liu, Z.; Lu, X. Self-Assembly-Induced Alternately Stacked Single-Layer MoS_2 and N-doped Graphene: A Novel van der Waals Heterostructure for Lithium-Ion Batteries. *ACS Appl. Mater. Interfaces* **2016**, *8*, 2372–2379. [CrossRef] [PubMed]
111. Jiao, J.; Du, K.; Wang, Y.; Sun, P.; Zhao, H.; Tang, P.; Fan, Q.; Tian, H.; Li, Q.; Xu, Q. N plasma treatment on graphene oxide-MoS_2 composites for improved performance in lithium ion batteries. *Mater. Chem. Phys.* **2020**, *240*, 122169. [CrossRef]
112. Zhou, J.; Qin, J.; Zhang, X.; Shi, C.; Liu, E.; Li, J.; Zhao, N.; He, C. 2D space-confined synthesis of few-layer MoS_2 anchored on carbon nanosheet for lithium-ion battery anode. *ACS Nano* **2015**, *9*, 3837–3848. [CrossRef] [PubMed]
113. Dinh, D.A.; Nguyen, T.L.; Cuong, T.V.; Hui, K.S.; Bui, T.H.; Wu, S.; Hui, K.N. Defect-Free MoS_2-Flakes/Amorphous-Carbon Hybrid as an Advanced Anode for Lithium-Ion Batteries. *Energy Fuels* **2021**, *35*, 3459–3468. [CrossRef]
114. Pan, Y.; Zhang, J.; Lu, H. Uniform Yolk–Shell MoS_2@Carbon Microsphere Anodes for High-Performance Lithium-Ion Batteries. *Chem. A Eur. J.* **2017**, *23*, 9937–9945. [CrossRef] [PubMed]
115. Wang, Y.; Ma, Z.; Chen, Y.; Zou, M.; Yousaf, M.; Yang, Y.; Yang, L.; Cao, A.; Han, R.P.S. Controlled Synthesis of Core–Shell Carbon@MoS_2 Nanotube Sponges as High-Performance Battery Electrodes. *Adv. Mater.* **2016**, *28*, 10175–10181. [CrossRef] [PubMed]
116. Zhou, Z.; Chen, F.; Wu, L.; Kuang, T.; Liu, X.; Yang, J.; Fan, P.; Fei, Z.; Zhao, Z.; Zhong, M. Heteroatoms-doped 3D carbon nanosphere cages embedded with MoS_2 for lithium-ion battery. *Electrochim. Acta* **2020**, *332*, 135490. [CrossRef]
117. Kong, J.; Zhao, C.; Wei, Y.; Lu, X. MoS_2 Nanosheets Hosted in Polydopamine-Derived Mesoporous Carbon Nanofibers as Lithium-Ion Battery Anodes: Enhanced MoS_2 Capacity Utilization and Underlying Mechanism. *ACS Appl. Mater. Interfaces* **2015**, *7*, 24279–24287. [CrossRef] [PubMed]
118. Hu, L.; Ren, Y.; Yang, H.; Xu, Q. Fabrication of 3D Hierarchical MoS_2/Polyaniline and MoS_2/C Architectures for Lithium-Ion Battery Applications. *ACS Appl. Mater. Interfaces* **2014**, *6*, 14644–14652. [CrossRef] [PubMed]
119. Zhang, D.; Zhang, W.; Zhang, S.; Ji, X.; Li, L. Synthesis of expanded graphite-based materials for application in lithium-based batteries. *J. Energy Storage* **2023**, *60*, 106678. [CrossRef]
120. Guan, P.; Zhou, L.; Yu, Z.; Sun, Y.; Liu, Y.; Wu, F.; Jiang, Y.; Chu, D. Recent progress of surface coating on cathode materials for high-performance lithium-ion batteries. *J. Energy Chem.* **2020**, *43*, 220–235. [CrossRef]
121. Lyu, Y.; Wu, X.; Wang, K.; Feng, Z.; Cheng, T.; Liu, Y.; Wang, M.; Chen, R.; Xu, L.; Zhou, J. An overview on the advances of $LiCoO_2$ cathodes for lithium-ion batteries. *Adv. Energy Mater.* **2021**, *11*, 2000982. [CrossRef]
122. Cui, C.; Li, X.; Hu, Z.; Xu, J.; Liu, H.; Ma, J. Growth of MoS_2@C nanobowls as a lithium-ion battery anode material. *RSC Adv.* **2015**, *5*, 92506–92514. [CrossRef]
123. Jiang, F.; Li, S.; Ge, P.; Tang, H.; Khoso, S.A.; Zhang, C.; Yang, Y.; Hou, H.; Hu, Y.; Sun, W.; et al. Size-tunable natural mineral-molybdenite for lithium-ion batteries toward: Enhanced storage capacity and quicken ions transferring. *Front. Chem.* **2018**, *6*, 389. [CrossRef] [PubMed]
124. Francis, M.K.; Rajesh, K.; Bhargav, P.B.; Ahmed, N. Binder-free phosphorus-doped MoS_2 flexible anode deposited on carbon cloth for high-capacity Li-ion battery applications. *J. Mater. Sci.* **2023**, *58*, 4054–4069. [CrossRef]
125. Zhao, Y.; Zhang, Y.; Yang, Z.; Yan, Y.; Sun, K. Synthesis of MoS_2 and MoO_2 for their applications in H_2 generation and lithium ion batteries: A review. *Sci. Technol. Adv. Mater.* **2013**, *14*, 043501. [CrossRef] [PubMed]
126. Liu, M.; Li, N.; Wang, S.; Li, Y.; Liang, C.; Yu, K. 3D nanoflower-like MoS_2 grown on wheat straw cellulose carbon for lithium-ion battery anode material. *J. Alloys Compd.* **2023**, *933*, 167689. [CrossRef]
127. Zhu, W.; Kamali, A.R. Green preparation of nanostructured β-MoO_3/hexagonal-shaped MoS_2/graphene with enhanced lithium-ion storage performance. *J. Alloys Compd.* **2023**, *932*, 167724. [CrossRef]
128. Salah, M.; Hall, C.; Francis, C.; Rollo-Walker, G.; Fabretto, M. Binary silicon-based thin-film anodes for lithium-ion batteries: A review. *J. Power Sources* **2022**, *520*, 230871. [CrossRef]
129. Li, L.; Zhang, D.; Deng, J.; Gou, Y.; Fang, J.; Cui, H.; Zhao, Y.; Cao, M. Carbon-based materials for fast charging lithium-ion batteries. *Carbon* **2021**, *183*, 721–734. [CrossRef]
130. Cheng, X.-B.; Zhang, Q. Dendrite-free lithium metal anodes: Stable solid electrolyte interphases for high-efficiency batteries. *J. Mater. Chem. A* **2015**, *3*, 7207–7209. [CrossRef]
131. Nzereogu, P.; Omah, A.; Ezema, F.; Iwuoha, E.; Nwanya, A. Anode materials for lithium-ion batteries: A review. *Appl. Surf. Sci. Adv.* **2022**, *9*, 100233. [CrossRef]
132. Hai, N.Q.; Kwon, S.H.; Kim, H.; Kim, I.T.; Lee, S.G.; Hur, J. High-performance MoS_2-based nanocomposite anode prepared by high-energy mechanical milling: The effect of carbonaceous matrix on MoS_2. *Electrochim. Acta* **2018**, *260*, 129–138. [CrossRef]
133. Zu, G.; Yang, Y.; Li, H.; Wang, J.; Fu, Y.; Wang, X.; Zhou, W.; Wang, J. The compactness of 2H-MoS_2 thin films determines their performance on lithium storage ability. *Mater. Charact.* **2023**, *196*, 112570. [CrossRef]
134. Guo, B.; Feng, Y.; Chen, X.; Li, B.; Yu, K. Preparation of yolk-shell MoS_2 nanospheres covered with carbon shell for excellent lithium-ion battery anodes. *Appl. Surf. Sci.* **2018**, *434*, 1021–1029. [CrossRef]

135. Zhao, L.; Wang, Y.; Wei, C.; Huang, X.; Zhang, X.; Wen, G. MoS_2-based anode materials for lithium-ion batteries: Developments and perspectives. *Particuology* **2024**, *87*, 240–270. [CrossRef]
136. Zeng, Z.; Zhang, X.; Bustillo, K.; Niu, K.; Gammer, C.; Xu, J.; Zheng, H. In situ study of lithiation and delithiation of MoS_2 nanosheets using electrochemical liquid cell transmission electron microscopy. *Nano Lett.* **2015**, *15*, 5214–5220. [CrossRef] [PubMed]
137. Wang, C.-J.; Zhu, Y.-L.; Zhang, T.; Tian, J.; Gao, F.; Zhao, Y.; Bu, X.-Y.; Quan, T. Competition between discharge reaction and side reaction for anode's lithium during internal short circuit in lithium-ion batteries. *J. Clean. Prod.* **2024**, *470*, 143280. [CrossRef]
138. Caputo, R.; Tekin, A.; Nesper, R. Topochemical Path in High Lithiation of MoS_2. *Z. Für Anorg. Und Allg. Chem.* **2019**, *645*, 309–316. [CrossRef]
139. Cheng, Y.; Nie, A.; Zhang, Q.; Gan, L.-Y.; Shahbazian-Yassar, R.; Schwingenschlogl, U. Origin of the phase transition in lithiated molybdenum disulfide. *ACS Nano* **2014**, *8*, 11447–11453. [CrossRef] [PubMed]
140. Shu, H.; Li, F.; Hu, C.; Liang, P.; Cao, D.; Chen, X. The capacity fading mechanism and improvement of cycling stability in MoS_2-based anode materials for lithium-ion batteries. *Nanoscale* **2016**, *8*, 2918–2926. [CrossRef] [PubMed]
141. Zhao, T.; Shu, H.; Shen, Z.; Hu, H.; Wang, J.; Chen, X. Electrochemical Lithiation Mechanism of Two-Dimensional Transition-Metal Dichalcogenide Anode Materials: Intercalation versus Conversion Reactions. *J. Phys. Chem. C* **2019**, *123*, 2139–2146. [CrossRef]
142. Zhu, Z.; Xi, S.; Miao, L.; Tang, Y.; Zeng, Y.; Xia, H.; Lv, Z.; Zhang, W.; Ge, X.; Zhang, H.; et al. Unraveling the Formation of Amorphous MoS_2 Nanograins during the Electrochemical Delithiation Process. *Adv. Funct. Mater.* **2019**, *29*, 1904843. [CrossRef]
143. Py, M.A.; Haering, R.R. Structural destabilization induced by lithium intercalation in MoS_2 and related compounds. *Can. J. Phys.* **1983**, *61*, 76–84. [CrossRef]
144. Cook, J.B.; Kim, H.-S.; Yan, Y.; Ko, J.S.; Robbennolt, S.; Dunn, B.; Tolbert, S.H. Mesoporous MoS_2 as a Transition Metal Dichalcogenide Exhibiting Pseudocapacitive Li and Na-Ion Charge Storage. *Adv. Energy Mater.* **2016**, *6*, 1501937. [CrossRef]
145. Kan, M.; Wang, J.Y.; Li, X.W.; Zhang, S.H.; Li, Y.W.; Kawazoe, Y.; Sun, Q.; Jena, P. Structures and phase transition of a MoS_2 monolayer. *J. Phys. Chem. C* **2014**, *118*, 1515–1522. [CrossRef]
146. Wang, L.; Zhang, Q.; Zhu, J.; Duan, X.; Xu, Z.; Liu, Y.; Yang, H.; Lu, B. Nature of extra capacity in MoS_2 electrodes: Molybdenum atoms accommodate with lithium. *Energy Storage Mater.* **2019**, *16*, 37–45. [CrossRef]
147. Zhu, Z.; Tang, Y.; Lv, Z.; Wei, J.; Zhang, Y.; Wang, R.; Zhang, W.; Xia, H.; Ge, M.; Chen, X. Fluoroethylene Carbonate enabling a robust LiF-rich solid electrolyte interphase to enhance the stability of the MoS_2 Anode for Lithium-ion storage. *Angew. Chem.* **2018**, *130*, 3718–3722. [CrossRef]
148. Yu, L.; Su, Q.; Li, B.; Huang, L.; Du, G.; Ding, S.; Zhao, W.; Zhang, M.; Xu, B. Pre-lithiated Edge-enriched MoS_2 nanoplates embedded into carbon nanofibers as protective layers to stabilize Li metal anodes. *Chem. Eng. J.* **2022**, *429*, 132479. [CrossRef]
149. Jiao, Y.; Mukhopadhyay, A.; Ma, Y.; Yang, L.; Hafez, A.M.; Zhu, H. Ion transport nanotube assembled with vertically aligned metallic MoS_2 for high rate lithium-ion batteries. *Adv. Energy Mater.* **2018**, *8*, 1702779. [CrossRef]
150. Nasir, M.Z.M.; Sofer, Z.; Ambrosi, A.; Pumera, M. A limited anodic and cathodic potential window of MoS_2: Limitations in electrochemical applications. *Nanoscale* **2015**, *7*, 3126–3129. [CrossRef] [PubMed]
151. Burse, S.R.; Tyagaraj, H.B.; Safarkhani, M.; Marje, S.J.; Gagankumar, S.K.; Al Ghaferi, A.; Alhajri, E.; Chodankar, N.R.; Huh, Y.S.; Han, Y.-K. Unleashing potential: Engineering advancements in two-dimensional MoS_2 for improved energy applications. *Adv. Compos. Hybrid Mater.* **2025**, *8*, 216. [CrossRef]
152. Mammeri, F.; Le Bourhis, E.; Rozes, L.; Sanchez, C. Mechanical properties of hybrid organic–inorganic materials. *J. Mater. Chem.* **2005**, *15*, 3787–3811. [CrossRef]
153. Rashidi, M.; Ghasemi, F. Thermally oxidized MoS_2-based hybrids as superior electrodes for supercapacitor and photoelectrochemical applications. *Electrochim. Acta* **2022**, *435*, 141379. [CrossRef]
154. Wang, R.; Wang, S.; Jin, D.; Zhang, Y.; Cai, Y.; Ma, J.; Zhang, L. Engineering layer structure of MoS_2-graphene composites with robust and fast lithium storage for high-performance Li-ion capacitors. *Energy Storage Mater.* **2017**, *9*, 195–205. [CrossRef]
155. Liu, C.; Bai, Y.; Zhao, Y.; Yao, H.; Pang, H. MoS_2/graphene composites: Fabrication and electrochemical energy storage. *Energy Storage Mater.* **2020**, *33*, 470–502. [CrossRef]
156. Jiang, L.; Lin, B.; Li, X.; Song, X.; Xia, H.; Li, L.; Zeng, H. Monolayer MoS_2–Graphene Hybrid Aerogels with Controllable Porosity for Lithium-Ion Batteries with High Reversible Capacity. *ACS Appl. Mater. Interfaces* **2016**, *8*, 2680–2687. [CrossRef] [PubMed]
157. Deng, Z.; Jiang, H.; Hu, Y.; Liu, Y.; Zhang, L.; Liu, H.; Li, C. 3D Ordered Macroporous MoS_2@C Nanostructure for Flexible Li-Ion Batteries. *Adv. Mater.* **2017**, *29*, 1603020. [CrossRef] [PubMed]
158. Zhang, L.; Lou, X.W. Hierarchical MoS_2 Shells Supported on Carbon Spheres for Highly Reversible Lithium Storage. *Chem. A Eur. J.* **2014**, *20*, 5219–5223. [CrossRef] [PubMed]
159. Chhowalla, M.; Shin, H.S.; Eda, G.; Li, L.-J.; Loh, K.P.; Zhang, H. The chemistry of two-dimensional layered transition metal dichalcogenide nanosheets. *Nat. Chem.* **2013**, *5*, 263–275. [CrossRef] [PubMed]
160. Ferrari, S.; Falco, M.; Muñoz-García, A.B.; Bonomo, M.; Brutti, S.; Pavone, M.; Gerbaldi, C. Solid-State Post Li Metal Ion Batteries: A Sustainable Forthcoming Reality? *Adv. Energy Mater.* **2021**, *11*, 2100785. [CrossRef]

161. Meng, R.; Wu, J.; Zhu, M.; Chang, M.; Zhang, N.; Cao, P.; Tian, F.; Yao, X. Two-Dimensional MoS_2 NS@$Li_7P_3S_{11}$ Composite Cathode for All-Solid-State Lithium Batteries. *ACS Appl. Energy Mater.* **2024**, *7*, 4603–4608. [CrossRef]
162. Marriam, I.; Tebyetekerwa, M.; Chen, H.; Chathuranga, H.; Motta, N.; Alarco, J.A.; He, Z.-J.; Zheng, J.-C.; Du, A.; Yan, C. Few-layer MoS_2 nanosheets with and without silicon nanoparticles as anodes for lithium-ion batteries. *J. Mater. Chem. A* **2023**, *11*, 2670–2678. [CrossRef]
163. Xu, R.-C.; Xia, X.-H.; Wang, X.-L.; Xia, Y.; Tu, J.-P. Tailored Li_2S–P_2S_5 glass-ceramic electrolyte by MoS_2 doping, possessing high ionic conductivity for all-solid-state lithium-sulfur batteries. *J. Mater. Chem. A* **2017**, *5*, 2829–2834. [CrossRef]
164. Chen, Y.; Song, B.; Tang, X.; Lu, L.; Xue, J. Ultrasmall Fe_3O_4 Nanoparticle/MoS_2 Nanosheet Composites with Superior Performances for Lithium Ion Batteries. *Small* **2014**, *10*, 1536–1543. [CrossRef] [PubMed]
165. Chen, B.; Liu, E.; Cao, T.; He, F.; Shi, C.; He, C.; Ma, L.; Li, Q.; Li, J.; Zhao, N. Controllable graphene incorporation and defect engineering in MoS_2-TiO_2 based composites: Towards high-performance lithium-ion batteries anode materials. *Nano Energy* **2017**, *33*, 247–256. [CrossRef]
166. Zhuang, W.; Li, L.; Zhu, J.; An, R.; Lu, L.; Lu, X.; Wu, X.; Ying, H. Facile Synthesis of Mesoporous MoS_2-TiO_2 Nanofibers for Ultrastable Lithium Ion Battery Anodes. *ChemElectroChem* **2015**, *2*, 374–381. [CrossRef]
167. Villevieille, C.; Wang, X.-J.; Krumeich, F.; Nesper, R.; Novák, P. MoS_2 coating on MoO_3 nanobelts: A novel approach for a high specific charge electrode for rechargeable Li-ion batteries. *J. Power Sources* **2015**, *279*, 636–644. [CrossRef]
168. Younis, M.W.; Akhter, T.; Yousaf, M.; Ali, M.; Naeem, H. Controlled dynamic variation of interfacial electronic and optical properties of lithium intercalated ZrO_2/MoS_2 vdW heterostructure. *J. Mol. Graph. Model.* **2024**, *127*, 108694. [CrossRef] [PubMed]
169. Shahmohammadi, A.; Dalvand, S.; Molaei, A.; Mousavi-Khoshdel, S.M.; Yazdanfar, N.; Hasanzadeh, M. Transition metal phosphide/ molybdenum disulfide heterostructures towards advanced electrochemical energy storage: Recent progress and challenges. *RSC Adv.* **2025**, *15*, 13397–13430. [CrossRef] [PubMed]
170. Zhang, X.; Li, J.; Han, L.; Li, H.; Wang, J.; Lu, T.; Pan, L. In-situ fabrication of few-layered MoS_2 wrapped on TiO_2-decorated MXene as anode material for durable lithium-ion storage. *J. Colloid Interface Sci.* **2021**, *604*, 30–38. [CrossRef] [PubMed]
171. Valizadeh, A.; Amirhosseini, M.H. Machine Learning in Lithium-Ion Battery: Applications, Challenges, and Future Trends. *SN Comput. Sci.* **2024**, *5*, 717. [CrossRef]
172. Lu, M.; Ji, H.; Chen, Y.; Gao, F.; Liu, B.; Long, P.; Deng, C.; Wang, Y.; Tao, J. Machine learning assisted layer-controlled synthesis of MoS_2. *J. Mater. Chem. C* **2024**, *12*, 8893–8900. [CrossRef]
173. Chen, X.; Liu, X.; Shen, X.; Zhang, Q. Applying machine learning to rechargeable batteries: From the microscale to the macroscale. *Angew. Chem.* **2021**, *133*, 24558–24570. [CrossRef]
174. Kilic, A.; Oral, B.; Eroglu, D.; Yildirim, R. Machine learning for beyond Li-ion batteries: Powering the research. *J. Energy Storage* **2023**, *73*, 109057. [CrossRef]
175. Lai, C.-H.; Lu, M.-Y.; Chen, L.-J. Metal sulfide nanostructures: Synthesis, properties and applications in energy conversion and storage. *J. Mater. Chem.* **2012**, *22*, 19–30. [CrossRef]
176. Chothe, U.; Ugale, C.; Kulkarni, M.; Kale, B. Solid-State Synthesis of Layered MoS_2 Nanosheets with Graphene for Sodium-Ion Batteries. *Crystals* **2021**, *11*, 660. [CrossRef]
177. Fang, Y.; Xiao, L.; Chen, Z.; Ai, X.; Cao, Y.; Yang, H. Recent Advances in Sodium-Ion Battery Materials. *Electrochem. Energy Rev.* **2018**, *1*, 294–323. [CrossRef]
178. Szkoda, M.; Ilnicka, A.; Trzciński, K.; Zarach, Z.; Roda, D.; Nowak, A.P. Synthesis and characterization of MoS_2-carbon based materials for enhanced energy storage applications. *Sci. Rep.* **2024**, *14*, 26128. [CrossRef] [PubMed]
179. Rahmatinejad, J.; Ye, Z. Advanced MoS_2 nanocomposites for post-lithium-ion batteries. *Chem. Eng. J.* **2024**, *500*, 156872. [CrossRef]
180. Chinnappan, N.; Punniyakoti, S. Emerging advances of 2D molybdenum disulfide (MoS_2) and their composites towards high-performance supercapacitors: A comprehensive review. *J. Energy Storage* **2024**, *102*, 114040. [CrossRef]
181. Joseph, N.; Shafi, P.M.; Bose, A.C. Recent Advances in 2D-MoS_2 and its Composite Nanostructures for Supercapacitor Electrode Application. *Energy Fuels* **2020**, *34*, 6558–6597. [CrossRef]
182. Liu, F.; Wang, T.; Liu, X.; Fan, L.-Z. Challenges and Recent Progress on Key Materials for Rechargeable Magnesium Batteries. *Adv. Energy Mater.* **2021**, *11*, 2000787. [CrossRef]
183. Kotobuki, M.; Yan, B.; Lu, L. Recent progress on cathode materials for rechargeable magnesium batteries. *Energy Storage Mater.* **2023**, *54*, 227–253. [CrossRef]
184. Liang, H.; Cao, Z.; Ming, F.; Zhang, W.; Anjum, D.H.; Cui, Y.; Cavallo, L.; Alshareef, H.N. Aqueous Zinc-Ion Storage in MoS_2 by Tuning the Intercalation Energy. *Nano Lett.* **2019**, *19*, 3199–3206. [CrossRef] [PubMed]